Book Section:
Ansell, RJ (2015) Characterization of the Binding Properties of Molecularly Imprinted Polymers. In: Mattiasson, B and Ye, L, (eds.) Molecularly Imprinted Polymers in Biotechnology. Advances in Biochemical Engineering/Biotechnology, 150 . Springer International Publishing , 51 - 93. ISBN 978-3-319-20728-5

https://doi.org/10.1007/10_2015_316

Characterization of the binding properties of Molecularly Imprinted Polymers

Richard J. Ansell

School of Chemistry, University of Leeds, Leeds LS2 9JT, United Kingdom

Abstract

The defining characteristic of the binding sites of any particular molecularly imprinted material is heterogeneity: that is, they are not all identical. Nonetheless, it is useful to study their fundamental binding properties, and to obtain average properties. In particular, it has been instructive to compare the binding properties of imprinted and non-imprinted materials.

This chapter begins by considering the origins of this site heterogeneity. Next, the properties of interest of imprinted binding sites are described in brief: affinity, selectivity, and kinetics. The binding/adsorption isotherm, the graph of concentration of analyte bound to a MIP versus concentration of free analyte at equilibrium, over a range of total concentrations, is described in some detail. Following this, the techniques for studying the imprinted sites are described (batch binding assays, radioligand binding assays, zonal chromatography, frontal chromatography, calorimetry, and others). Thereafter, the parameters which influence affinity, selectivity and kinetics are discussed (solvent, modifiers of organic solvents, pH of aqueous solvents, temperature). Finally, mathematical attempts to fit the adsorption isotherms for imprinted materials, so as to obtain information about the range of binding affinities characterizing the imprinted sites, are summarized.

1. Properties of molecularly imprinted binding sites

The defining characteristic of molecularly imprinted binding sites is heterogeneity: that is, they are not all identical (in the manner of monoclonal antibodies, or synthetic receptors such as crown ethers), but differ in the exact spatial arrangement of functional groups, the access to the site, the polarity of the immediate environment etc. Thus, they are more analogous to polyclonal antibodies, where different sequences give different structures at the antigen binding sites. In the case of non-covalently imprinted materials, much of this heterogeneity arises from the fact, that the monomer-template interactions are governed by equilibria such that a range of monomer-template complexes, along with free, uncomplexed monomer, are present in the pre-polymerisation mixture (Figure 1a), and this diversity is pre-

served in the macromolecular material after polymerization (Figure 1b). Processing of the material (e.g. by grinding and sieving), removal of the template, and exchange of the polymerization solvent with a different solvent to study the binding properties, can all lead to further heterogeneity by damaging binding sites, sites collapsing on template removal, and locally variable swelling/collapse of the polymer in a different solvent (figure 1c).

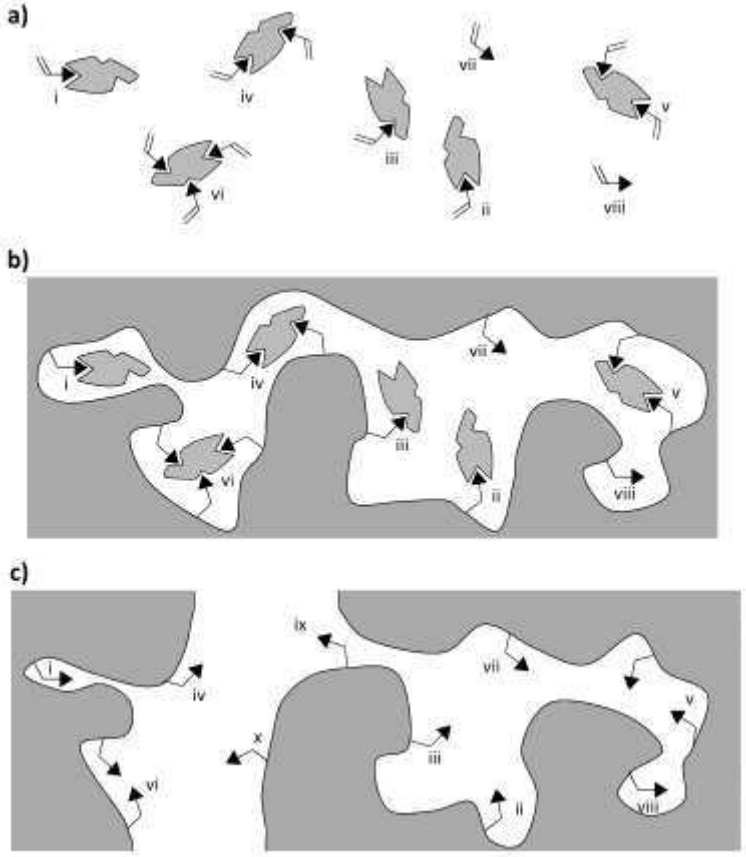

Fig. 1. 2-dimensional cartoon representation of the origins of heterogeneity in molecularly imprinted binding sites. a) The species present in the pre-polymerisation equilibria. Grey shape represents the template, black triangles represent monomer. Cross-linker not shown, for clarity. The template has three distinct sites to interact with monomer and a 2:1 ratio of monomer:template is shown. i and ii are 1:1 complexes, iii is a 1:1 complex but with a different form of monomer-template interaction, iv and v are 2:1 complexes, vi is a 3:1 complex, vii and viii are free uncomplexed monomer. b) The structure post-polymerisation. Previously equivalent structures i and ii have yielded different binding sites due to different outer-sphere interactions i.e. different polymer backbone conformation, and different site accessibility. Likewise iv and v, and vii and viii. c) The structure after polymer processing, template removal, and solvent exchange. Site i has collapsed after template removal. Sites iv and vi have been damaged by polymer fracturing (and generated two new weak and non-selective sites ix and x). All sites have been modified by the swelling of the polymer.

The binding site heterogeneity is usually acknowledged at least in so far as authors discuss 'specific' and 'non-specific' binding to imprinted materials. At the simplest level, we might consider sites arising from any form of monomer-template complex in the pre-polymerisation mixture (i-vi in figure 1) to be 'specific': these are expected to have a higher affinity for the template (and similar structures), and to be more selective in not binding dissimilar ones (due to 'the precise arrangement of the functional groups' and 'shape selectivity'). Sites arising from free, non-complexed monomer in the pre-polymerisation mixture (vii and viii in figure 1) are proposed to give 'non-specific' sites: these are expected to have lower affinity for the template and to bind other species indiscriminately, just as a polymer with randomly arranged functional monomer (e.g. a non-imprinted polymer, prepared in the absence of template) would be expected to behave. However, whilst this simplistic dichotomy between 'specific sites' and 'non-specific sites' (or 'imprinted sites' and 'non-imprinted sites') can be useful, it certainly does not capture the full picture, which is of a continuous spectrum of sites from weaker binding, less selective, to stronger binding, more selective.

The diversity of species in the pre-polymerisation mixture will be even greater than suggested in Figure 1a if there is more than one type of monomer present, or if the monomer or the template are capable of interactions with the cross-linker, or if 'clusters' of template are present [1-4]. The thesis that the pre-polymerisation species (Figure 1a) are precisely replicated in the polymerized material (Figure 1b) is probably naïve, several works having suggested that these structures change during the course of polymerization [5]: however, the broader principle that diversity is preserved or enhanced is certainly valid (e.g. due to the polymeric chains being folded in different ways around different sites, 'outer sphere' interactions for each site will be different).

Although the model in Figure 1 particularly illustrates the case for non-covalent imprinting of organic monomers, which polymerise into cross-linked chains, the principle is applicable to all forms of imprinting:

- *Stoichiometric non-covalent/covalent/semi-covalent/metal-mediated imprinting*: although these strategies all involve entirely (or almost entirely) 1:1 complexes of monomer and template, such that there are (in theory) no free monomers, nor any 2:1 or higher complexes, diversity will still be generated due to the different 'outer-sphere' interactions in the polymerized material, different site accessibility, plus changes due to site damage in polymer processing, site collapse, and swelling/collapse of the polymer after solvent exchange.

- *Sol-gel imprinting*: the monomeric species may form more than one covalent bond with the cross-linker, the cross-linker may be multivalent, and the polymerisation ionic rather than free-radical, but the principles of figure 1 remain. The cross-linked gel is an amorphous material, even if it is inorganic, without crystalline form, so the structure is just as heterogeneous.

- *Surface imprinting*: the 2-dimensional nature of figure 1 demonstrates clearly how the same principles will apply in imprinting in 2-dimensions on a surface. When the monomer-template interaction is non-covalent, a range of monomer-template complexes will be present initially. If the imprinting is done on a homo-

geneous surface and the monomers form a monolayer, then the difference in 'outer-sphere' environments of the binding sites will certainly be limited. However, even with stoichiometric monomer-template interactions and a monolayer approach, there will still be differences in the exact orientation of functional groups on the surface and defects in the structure.

- *Pre-polymer imprinting*: polymer chains can be 'fixed' in the presence of a template by phase-inversion precipitation [6] or solvent evaporation [7] the chains are cross-linked physically but not chemically. These approaches are closely related to 'bioimprinting' in proteins whose structure is 'frozen' by lyophilisation or chemical cross-linking in the presence of a template[8]. A range of structures will be present initially as the template interacts with the linear polymer, and the heterogeneity of folded structures formed during precipitation will be no less than when the polymer chains cross-link covalently.

A great deal of effort has been invested in reducing the heterogeneity of the pre-polymerization mixture for non-covalent imprinting as represented in figure 1a, by studying the monomer-template equilibria to optimize the monomer-template ratio [9], by choosing/creating new monomers such that the monomer-template interaction is as strong as possible [10-15], and at the simplest level by choosing a solvent in which the interactions are strongest. However, diversity in the binding sites cannot be avoided, for the same reasons that it is present even in covalent imprinting.

For some applications, some binding site diversity (for example, a range of different binding site affinities) may be useful [16] however in most applications it is considered a hindrance (for example in zonal chromatography, where it leads to the tailing of chromatographic peaks and consequently poor column efficiency and resolution), and it is perceived by the wider scientific community as a limitation. Certainly, in order to design imprinted materials for specific applications, it is essential to have an understanding of the binding site heterogeneity and how it arises.

When characterizing the binding properties, there are three properties of particular interest:

- *Binding site affinity*: the binding/unbinding of analyte to/from the imprinted binding sites can be represented as an equilibrium:

$$\text{free analte} + \text{binding site} \overset{K_a}{\leftrightarrow} \text{bound analyte} \tag{1}$$

Where K_a is the association constant (in mol^{-1} L), and if all sites were identical then K_a might be expressed as

$$K_a = \frac{n_{bound}}{n_{empty} \times F} = \frac{1}{K_d} \tag{2}$$

where K_d is the dissociation constant (in mol L^{-1}), n_{bound} is the mols of bound analyte, F is the concentration of free analyte in solution (in mol L^{-1}) and n_{empty} is the mols of empty binding sites. Unfortunately, because the binding sites are not

equivalent (as outlined above), each site (in the same material) will have a different K_a. The quotient (n_{bound} / (n_{empty} × F)) will change even as the total amount of analyte changes. Moreover the number of empty binding sites is not a parameter that can be readily measured, hence the calculation of association constants for a MIP polymer is not straightforward (see sections 2 and 5). Instead, the binding under a specified set of conditions is usually expressed simply as n_{bound}, or as %bound ($n_{bound}/n_{analyte}$×100%, where $n_{analyte}$ is the total mols of analyte present in the experiment), or as a distribution ratio D (in L g^{-1})

$$D = \frac{B}{F} = \frac{n_{\text{bound}}/M_{\text{MIP}}}{n_{\text{free}}/V} \tag{3}$$

where B is the concentration of bound analyte (in mol g^{-1}), M_{MIP} is the mass of MIP polymer (in g), V is the volume of solution in which the material is incubated and n_{free} is the amount of free analyte in solution (in mol) such that

$$n_{\text{analyte}} = n_{\text{bound}} + n_{\text{free}} \tag{4}$$

- *Binding site selectivity*: the presence of 'imprinted sites' is usually verified by comparing an imprinted polymer with one made under the same conditions but in the absence of template (the non-imprinted polymer, NIP). One commonly calculated parameter is the *imprinting factor, IF*, best defined as the ratio of the distribution ratio for a particular analyte, under a particular set of conditions, on the imprinted polymer, to the distribution ratio for the same analyte, under identical conditions, on the NIP:

$$IF = \frac{D_{\text{MIP}}}{D_{\text{NIP}}} = \frac{B_{\text{MIP}}/F_{\text{MIP}}}{B_{\text{NIP}}/F_{\text{NIP}}} = \frac{n_{\text{bound, MIP}}/n_{\text{free, MIP}}}{n_{\text{bound, NIP}}/n_{\text{free, NIP}}} \tag{5}$$

where the volume V is the same for the MIP as for the NIP, and M_{MIP} is the same as M_{NIP}. The *IF* should have a value greater than 1, the higher the value the greater the difference between the imprinted and non-imprinted case. It is important to bear in mind, however, that the NIP may bind less analyte than the MIP because monomer self-association occurs to a higher extent in the NIP and reduces the number of free functional groups. Moreover, Baggiani *et al.* have suggested that when optimizing MIP composition, the MIP with the highest affinity and selectivity towards its template usually corresponds to a NIP which binds the template strongly too[17]. Hence, a high *IF* may not be the best indicator of a useful MIP: comparing the binding of the template-analyte to a MIP with the binding of the template-analyte to a polymer imprinted with a different template may be a better measure of successful imprinting. Further, a high *IF* does not prove that the 'imprinted sites' are selective. In order to demonstrate this, the rebinding of the template (or the target analyte, if different) to the MIP must be compared with the binding of a competitor, again under identical conditions:

$$\alpha_{\text{competitor 1}} = \frac{D_{\text{analyte, MIP}}}{D_{\text{competitor 1, MIP}}} = \frac{B_{\text{analyte, MIP}}/F_{\text{analyte, MIP}}}{B_{\text{competitor 1, MIP}}/F_{\text{competitor 1, MIP}}} \quad (6)$$

The *selectivity factor*, α, should have a value greater than 1, and high values of α for a range of competitors provide evidence of selectivity.

- *Binding/unbinding kinetics*: The binding/rebinding process can be represented as

$$\text{free analte} + \text{binding site} \xrightarrow{k_1} \text{bound analyte} \quad (7)$$

where the rate constant k_1 (in mol^{-1} L s^{-1}) is such that

$$\frac{\mathrm{d}n_{\text{bound}}}{dt} = k_1 \times n_{\text{empty}} \times F \quad (8)$$

The unbinding process is represented as

$$\text{bound analyte} \xrightarrow{k_{-1}} \text{free analte} + \text{binding site} \quad (9)$$

where the rate constant k_{-1} (in s^{-1}) is such that

$$\frac{\mathrm{d}n_{\text{empty}}}{dt} = -\frac{\mathrm{d}n_{\text{bound}}}{dt} = k_{-1} \times n_{\text{bound}} \quad (10)$$

from which it follows that, under conditions of dynamic equilibrium

$$k_{-1} \times n_{\text{bound}} = k_1 \times n_{\text{empty}} \times F \quad (11)$$

and so

$$\frac{n_{\text{bound}}}{n_{\text{empty}} \times F} = \frac{k_1}{k-1} = K_{\text{a}} = \frac{1}{K_{\text{d}}} \quad (12)$$

Unfortunately, just as every different site on the imprinted material has a different association constant K_a, so it will also have different on (k_1) and off (k_{-1}) rate constants. Nonetheless, under a specific set of conditions it is possible to measure *effective* constants, K_a', k_1' and k_{-1}'. The rate constants for binding and unbinding on a MIP may be considered to be governed by mass transfer, that is, the transfer between the solution phase and the solid phase. This can be quite slow, because of the need for analyte to diffuse through the (albeit usually porous) solid material. Kinetics are usually faster for surface imprinted and thin-film imprinted materials than for monolithic materials, or particles where the binding sites are in the interior.

2. The binding/adsorption isotherm

2a. Collecting experimental data

Although frequently the binding of analyte is reported as n_{bound}, % bound or D under a single set of conditions, this is a poor way to characterise MIP binding. Each of these values will vary, even for the same combination of polymer, analyte and solvent, if $n_{analyte}$, V or M_{MIP} are changed. This will effect both the binding to MIP and to a control polymer, and binding of competitors, such that IF and α will also change with $n_{analyte}$, V and M_{MIP} [18,19]. Moreover, comparison between different MIPs is extremely difficult if binding is only recorded under a single set of conditions. Both Allender *et al.* [20] and Horvai *et al*. [18,19] have blamed the common use of single-point characterization for the confusion of many researchers from other fields when approaching the molecular imprinting literature.

According to both of these groups (and the current author), a far more useful way to characterize analyte binding is to measure/calculate values of the bound concentration B and free concentration F for a fixed amount of polymer and range of concentrations of added analyte: the graph of B *versus* F yields a *binding isotherm* as illustrated in Figure 2. This can be achieved in different ways, the simplest being to vary $n_{analyte}$ while V and M_{MIP} are kept constant, then, once equilibrium is achieved, measure F and calculate B. This method is commonly referred to as a *batch binding* or *batch rebinding* assay – it and other methods to derive the isotherm are discussed in section 3. Using $B = n_{bound}/ M_{MIP}$ and equation 4, B can be calculated from $n_{analyte}$ and F:

$$B = \frac{n_{analyte} - n_{free}}{M_{MIP}} = \frac{n_{analyte}}{M_{MIP}} - \frac{V}{M_{MIP}} \times F \qquad (13)$$

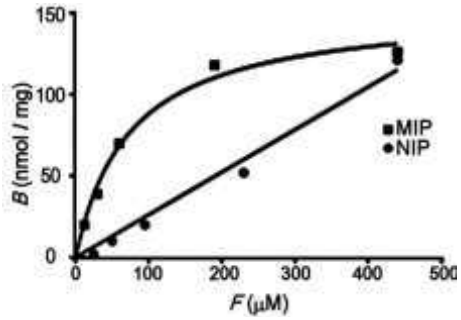

Fig. 2. A typical standard equilibrium bound (nmoles/mg)/free (μM) isotherm for a molecularly imprinted polymer (MIP) and a control non-imprinted polymer (NIP). In this example, the data describe binding isotherms for a propranolol imprinted poly(ethyleneglycoldimethacrylate-co-methacrylic acid) MIP and its corresponding NIP. Polymers were prepared by precipitation polymerisation[21]. Figure reproduced with permission from [20].

The data points may be connected by curves as shown in Figure 2, either empirically or based on a particular model of the type of binding sites present, as discussed in section 2b. 'Isotherm' refers to the temperature being kept constant: binding will change with temperature so it is important that all measurements are made at a constant temperature (and that the temperature is reported), just as it is important that the solution conditions (solvent, buffer, pH etc.) are also the same for all points on the experimental isotherm.

The experimental isotherm should ideally be derived from as many measurements, covering as wide a range of $n_{analyte}$ as possible. The isotherm for a MIP is not expected to be linear: rather, it usually flattens off at high F as in figure 2. This indicates saturation: all of the binding sites on the MIP are occupied so that B can increase no further even if more analyte is added to solution. The curvature of the binding isotherm can only be properly visualized if a wide enough range of concentration is studied.

Commonly, binding to a NIP (made under identical conditions and with identical constitution to the MIP except for the absence of the template molecule) is used as an indicator of non-specific binding (though this model is slightly naïve, as discussed in section 1). The NIP is considered to possess functional groups randomly arranged on its surface, and these interact with the analyte and cause it to bind to some extent, although (hopefully) more weakly than it does to the MIP. The difference in binding to the MIP and the NIP is attributed to specific binding i.e. the additional binding which occurs due to the presence of selective imprinted sites. For applications where selectivity for the analyte is important, efforts are usually made to maximize the specific binding i.e. the difference between the MIP and the non-imprinted control.

For consistency and ease of comparison, it is important that the isotherm is indeed expressed as a plot of B vs F. Other representations (e.g. with %bound or n_{bound} on the y-axis, and/or with the total concentration of analyte $n_{analyte}/V$, or just n_{total} on the x-axis) are less useful for direct comparison, and unhelpful if parameters such as M_{MIP} or V are not given. Whereas F may indeed be similar to the total concentration of analyte when the %bound is very small (because binding is extremely weak and/or because M_{MIP} is small compared to the amount of analyte), these quantities will be different when %bound increases, and the visualization of B vs F is far more useful than B vs total concentration as we shall see below.

One benefit of expressing the isotherm as B vs F and fitting data to an empirical curve is that we can draw, on the same graph, a straight line to represent the range of possible values for B and F given particular values of $n_{analyte}$, V and M_{MIP}[20]. This 'line of ligand conservation' is simply equation 13, and its y-

intercept is the limiting value of B if all the analyte binds while its x-intercept is the limiting value of F if none of the analyte binds.

For example figure 3 combines the isotherm with two straight lines representing different combinations of $n_{analyte}$, V and M_{MIP}. Where the straight line intersects the empirical isotherm gives the expected values of B and F under these conditions. Under the theoretical conditions of experiment 1, the MIP is expected to give $B \sim 92$ nmol mg^{-1} and $F \sim 110$ μmol dm^{-3} and the NIP $B \sim 52$ nmol g^{-1} and $F \sim 195$ μmol dm^{-3}. These values correspond to D for the MIP ~ 0.84 mL mg^{-1} and for the NIP ~ 0.27 mL mg^{-1}, giving an IF of ~3.1.

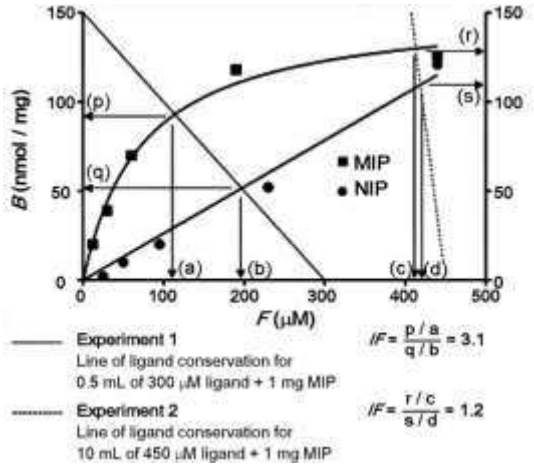

Fig. 3. An example of how distribution ratio (D) and imprinting factor (IF) are influenced by experimental parameters of ligand concentration, incubation volume and polymer mass. In Experiment 1, 0.5 ml of 300 μM ligand and 1 mg of polymer results in an IF of 3.1 whereas in Experiment 2, for 1 mg of the same MIP and NIP, a larger volume (10 ml) of 450 μM ligand solution gives an IF of 1.2. Figure reproduced with permission from [20].

Under the theoretical conditions of experiment 2 (in figure 3) where $n_{analyte}$ is much higher than experiment 1, the MIP is expected to give $B \sim 128$ nmol mg^{-1} and $F \sim 410$ μmol dm^{-3} and the NIP $B \sim 110$ nmol g^{-1} and $F \sim 420$ μmol dm^{-3}. These values correspond to D for the MIP ~ 0.31 mL mg^{-1} and for the NIP ~ 0.26 mL mg^{-1}, giving an imprinting factor of ~1.2. Thus, the model described in figure 3 helps illustrate and explain how, as $n_{analyte}$ increases relative to M_{MIP}:

- n_{bound} increases but, due to the curvature of the MIP isotherm, not as rapidly as $n_{analyte}$. Hence
- D_{MIP}, falls. Whilst
- D_{NIP} does not change so much, because the isotherm for the NIP is more linear. Hence
- IF decreases.

Therefore, to obtain a good IF in single point experiments, measurements are usually made with a very low ratio of $n_{analyte}$ to M_{MIP}. However, this may not re-

flect the conditions under which the MIP is intended to be used in a real application.

2b. Fitting the experimental data to a model

Where sufficient data points are collected and the errors are shown to be sufficiently low, data points on the binding isotherm may be fitted to a curve which can be either empirically based, or based on a theoretical model of the number of binding sites and their binding affinities. In figure 2, the isotherm is fitted to an arbitrary exponential function $B=129.7(1-e^{-0.01132F})$.

When the flattening of the curve at high values of F is clear, as it is in figure 2, it is possible to measure two empirical parameters B_{max}', which is the value of B when all of the binding sites are occupied and must usually be extrapolated, and K_d' which is the value of F (free analyte concentration) at which $B = 0.5\times B_{max}'$. From figure 2, values are obtained of $B_{max}' = 130$ nmol mg^{-1} and $K_d' = 61$ μM. Allender *et al*. [20] have suggested that B_{max}' and K_d' should be used commonly as a measure of the affinity of a MIP, and have conducted a meta-analysis of data on 47 MIPs from different publications between 2004 and 2008, which suggests that B_{max}' values commonly range between ~1 nmol and ~ 1 μmol per mg of polymer, while K_d' values commonly range between ~1 μM and 8 mM.

In order to understand the imprinting process better and improve future design of MIPs, researchers have fitted MIP adsorption isotherms to various theoretical models of the number of binding sites and their binding affinities (for a review, see [22]). The features of the models used are summarized in Table 1.

Model name	Equation	Classes of sites?	Linearises?	Saturates?
Langmuir	$B = \frac{F \times B_{\max}}{K_d + F}$	One, homogeneous	Yes	Yes
Bis-Langmuir	$B = \frac{F \times B_{\max 1}}{K_{d1} + F} + \frac{F \times B_{\max 2}}{K_{d2} + F}$	Two	No	Yes
Tri-Langmuir	$B = \frac{F \times B_{\max 1}}{K_{d1} + F} + \frac{F \times B_{\max 2}}{K_{d2} + F} + \frac{F \times B_{\max 3}}{K_{d3} + F}$	Three	No	Yes
Freundlich	$B = A \times F^m$	Continuous distribution – infinite number of v weak sites decaying to few v strong ones	Yes	No
Langmuir-Freundlich	$B = \frac{B_{\max} \times a \times F^m}{1 + a \times F^m}$	Gaussian distribution with clear maximum.	Yes, but requires estimation of $B_{\max}$	Yes

Table 1. Models used to fit experimental MIP adsorption isotherms.

The simplest (and most optimistic) model used has been the Langmuir isotherm, which assumes that all binding sites are identical, with a binding (association) constant K_a and dissociation constant $K_d = 1 / K_a$. From the equation in Table 1, it may be seen that when F=K_d then $B = 0.5 \times B_{max}$. Thus the empirical constants B_{max}' and K_d' described above are interpreted, in the Langmuir model, as the density of binding sites and the dissociation constant of those sites. Experimental values of B/F may be fitted to the isotherm using graph-fitting software, for example figure 4 shows data for caffeine binding to a caffeine-imprinted polymer fitted to the Langmuir isotherm using OriginPro™. Values are obtained from the data fit of B_{max}=(47±1) nmol g^{-1} and K_d = (2650±140) μM.

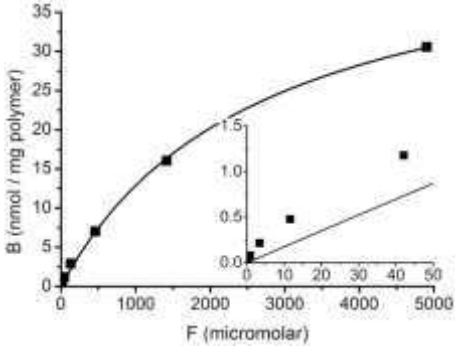

Fig. 4. Experimental *B*-*F* data for a caffeine-imprinted MIP determined by radioassay using the binding of ^{14}C-caffeine probe[23]. Assays performed in 1 mL volume of heptane/THF (3:1 v/v) using 8 mg of MIP and varying amounts of unlabelled caffeine. Data fitted to Langmuir isotherm using OriginPro™. Inset magnifies data at low *F*.

Prior to the availability of simple graph-fitting software, various approaches were used in which the Langmuir isotherm was linearized, to give a straight-line equation where y and x correspond to combinations of B and F. Best known of these is the Scatchard plot, where B/F is plotted against B. The Langmuir equation can be rearranged to show

$$\frac{B}{F} = -\frac{1}{K_d} \times B + \frac{B_{max}}{K_d} \quad (14)$$

Hence, a plot of B/F against B should be a straight line with gradient $-1/K_d$ and y-intercept B_{max}/K_d. Figure 5 shows the corresponding representation of the same data as in figure 4:

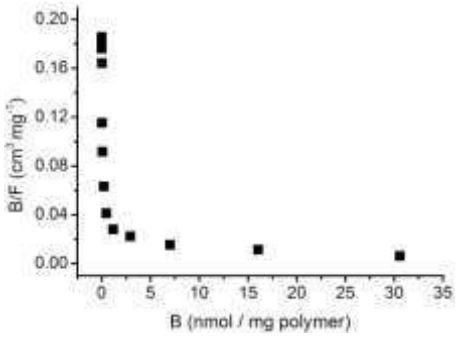

Fig. 5. Scatchard plot for binding data for a caffeine-imprinted MIP determined by radioassay using the binding of ^{14}C-caffeine probe, same conditions as figure 4 [23].

The data do not fit a straight line, confirming the inappropriateness of the Langmuir model in this case. However, it does appear (and is frequently observed with MIPs) that the Scatchard plot could be fitted with two separate straight lines – one line passing through the 7 points at lowest B values and another through the 3 points at highest B values. This approach is often taken, with the gradients and intercepts of the two lines being used to derive two sets of B_{max} and K_d values – one attributed to 'strong' binding sites and the other to 'weak' binding sites. However, this yields poor estimates of the parameters (see reference [24]).

The bi-Langmuir isotherm (table 1) is a model with two classes of binding sites (one with B_{max1} and K_{d1}, the other with B_{max2} and K_{d2}). This expression cannot be linearized in any combination of B and F, but non-linear graph-fitting software can be used to fit data. It was used initially by Mosbach *et al*. to fit isotherms obtained in MIP radioligand binding assays [25,26] and has been very widely applied since (e.g. [27-30]). Figure 6 shows the same data as in figure 4, fitted to the bi-Langmuir isotherm: the fit is much better, particularly at low F values. The fitted parameters are B_{max1} = (1.09±0.16) nmol g^{-1} and K_{d1} = (30.4±10.9) μM, B_{max2} = (48.8±0.4) nmol g^{-1} and K_{d2} = (3220±90) μM.

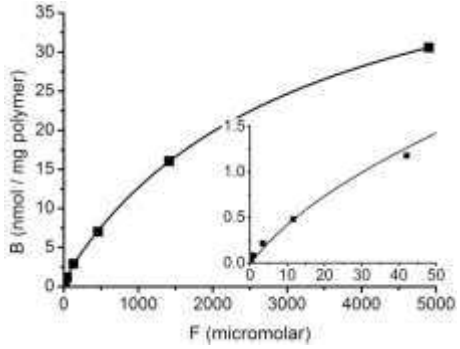

Fig. 6. Experimental *B*-*F* data for a caffeine-imprinted MIP as in figure 4 [23]. Data fitted to bi-Langmuir isotherm using OriginPro™. Inset magnifies data at low *F*.

The bi-Langmuir model is appealing, as it reflects the simplistic picture of specific, imprinted sites (the stronger binding sites, of which there are but few, in this case described by $B_{max1}$and K_{d1}), and the non-specific, non-imprinted sites (the weaker sites, of which there are relatively many, in this case described by $B_{max2}$and K_{d2}). Variations such as tri- (table 1) and tetra-Langmuir isotherms can be created by adding third and fourth terms to the equation, describing additional classes of sites: however it is important to acknowledge that adding additional parameters will inherently improve the fit between any model and data, and the inclusion of these additional parameters is only justified if the improvement in the fit is statistically significant as proven, for instance, by use of an *F*-test [22].

Models with two, three or even more classes of sites remain an oversimplification of the real situation in most cases, where there is likely to be a broad range of binding sites, each with slightly different conformations of functional groups and slightly different arrangements of polymeric chains, so that a more-or-less continuous range of binding sites with varying K_d values is more realistic.

An isotherm model which allows for a continuous range of binding sites with different affinities is the Freundlich isotherm (table 1). A (cm^3 mg^{-1}) and m (dimensionless) are empirical constants. m can be interpreted as a measure of site heterogeneity (m = 1 corresponding to homogeneous sites), and both parameters may be related to the binding site densities and dissociation constants, but non-trivially (section 5). In the case of the data from figure 4, the Freundlich isotherm fits rather poorly (figure 7), giving $A = (0.19 \pm 0.03)$ cm^3 mg^{-1} and $m = 0.60 \pm 0.02$.

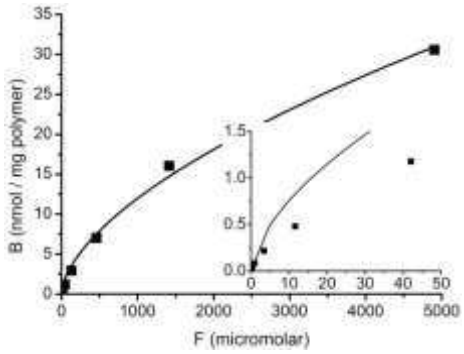

Fig. 7. Experimental *B*-*F* data for a caffeine-imprinted MIP as in figure 4 [23]. Data fitted to Freundlich isotherm using OriginPro™. Inset magnifies data at low *F*.

Although the Freundlich isotherm fits poorly in this case, it has been fitted more successfully to data from other MIPs, being used first by Guiochon *et al*. [29], and subsequently by the groups of Shimizu [31-33], Spivak [5] and many others. However, it does have some disadvantages, in comparison with other binding models [33]:

- it does not allow for binding saturation (i.e., however high *F* is increased, the isotherm predicts that more analyte can bind to the polymer indefinitely)
- the distribution of binding sites underlying the model is an exponentially decaying distribution, which predicts an infinite number of binding sites with K_d=0.

One advantage of the Freundlich isotherm is that it can be linearized, as in equation 15, such that the graph of log*B* vs log*F* has gradient *m* and intercept log *A*:

$$\log B = \log A + m \times \log F \tag{15}$$

When the data from figure 4 are transformed and plotted in this way (figure 8) the line of best fit yields A = (0.068±0.005) cm^3 mg^{-1} and m = 0.762±0.015. The discrepancy between these values and those obtained above for non-linear fitting of the data in figure 7 directly, reflects the fact that non-linear fitting of the raw data effectively weights the higher *F* data points more, while linear fitting of the the log-log plot weights the lower *F* data points more.

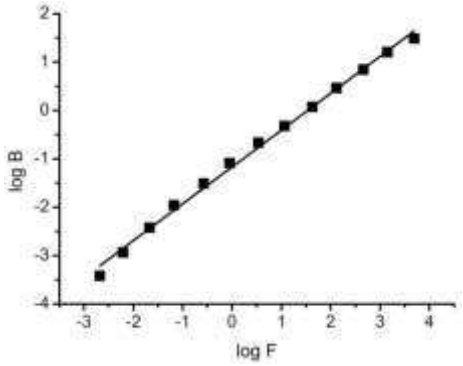

Fig. 8. Log-log plot of B-F data for a caffeine-imprinted MIP as in figure 4 [23]. Data fitted to straight line using OriginPro™.

The fourth commonly-applied model is the Langmuir-Freundlich isotherm (table 1) which was first applied to MIP binding data by Shimizu *et al.*[34], and has since been used by the groups of Martin-Esteban [35-37], Tovar [27], Diaz-Garcia [38] and many others. As in the Freundlich isotherm, a (dm^3 μmol^{-1}) and m (dimensionless) are empirical constants, which may be related to the binding site densities and dissociation constants, but non-trivially (section 5). When $m = 1$, the equation reduces to the Langmuir isotherm, whilst when F is extremely small, it reduces to the Freundlich isotherm (with $A = B_{max} \times a$). The equation is equivalent to the Hill equation, used in biochemistry, in which the coefficient m indicates the co-operativity of binding ($m>1$ indicates positive co-operativity, while $m<1$ indicates negative co-operativity). The Langmuir-Freundlich isotherm does saturate, such that B_{max} is the maximum density of bound analyte at very high F. It can also be shown that the concentration of free ligand at which $B = 0.5 \times B_{max}$ is given by $K_d' = (a)^{-1/m}$.

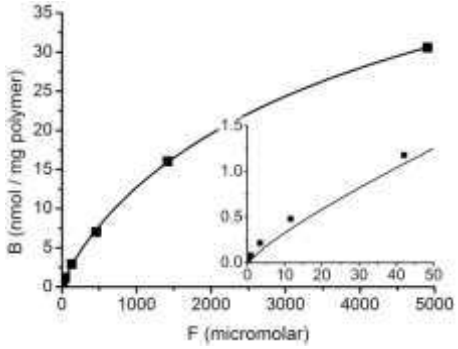

Fig. 9. Experimental *B-F* data for a caffeine-imprinted MIP as in figure 4 [23]. Data fitted to Langmuir-Freundlich isotherm using OriginPro™. Inset magnifies data at low F.

Fitting the data from figure 4 to the Langmuir-Freundlich isotherm yields B_{max} (60.9±3.2) nmol mg^{-1}, a = (7.69±0.87)×10^{-4} dm^3 μmol^{-1} and m = 0.845±0.021, hence $K_d{}'$ = 4840±570 μmol dm^{-3}. The fit is better than for the Freundlich isotherm though not, in this case, as good as for the bi-Langmuir isotherm (figure 9). The Langmuir-Freundlich isotherm also has the advantage that it may be linearized in the form

$$\ln \frac{B}{B_{max}-B} = \ln a + m \times \ln F \tag{16}$$

Since B_{max} is unknown, it must be estimated from the B-F data and systematically optimized until the plot of ln(B/(B_{max}-B)) vs ln$F$ gives the best straight line possible.

3. Methods for the characterization of imprinted binding sites

3a. Batch binding studies

The simplest possible experiment to characterize the properties of an imprinted material involves incubating a known mass of material (M_{MIP}, in g), with a known quantity of analyte ($n_{analyte}$, in mol) in a known volume of solvent (V, in L or mL). Once equilibrium has been reached (minutes, or hours, depending on the nature of the material), some will have bound to the material and some remains free in solution (equation 1). The material is separated from the solution and the free concentration F remaining in solution is measured. It is usually simpler (and more reliable) to measure F (from which n_{free} may be calculated) rather than B (which can then be calculated using equation 13).

In early work, Wulff *et al*. performed batch-binding experiments e.g. with racemic 4-nitrophenyl-mannopyranoside binding to a 4-nitrophenyl-α-D-mannopyranoside-imprinted vinylphenylboronic acid-co-DVB polymer. [39]. However, the batch binding method was first applied to derive MIP adsorption isotherms by Shea *et al*. [40] but has been used subsequently in hundreds of publications, inter alia [27,35,38,41-47].

The measurement of F must be as accurate and precise as possible, particularly if F is only slightly less than the total concentration, since B must be calculated from F as in equation 13. The experiment should be designed so as to minimise the error in the measured F. Spectroscopic quantification e.g. by absorbance at a single wavelength may suffer from interferences e.g. by any species released from the polymer. Since such a method is not selective, it is preferable to quantify F by a selective method e.g. HPLC. When the analyte is the same as the template molecule, bleeding of template from the polymer will distort the results at low $n_{analyte}$,

hence it is essential that the MIP is washed exhaustively before characterization. To check for the absence of error due to template bleeding, a control experiment where MIP is incubated in the assay solvent with $n_{analyte}$=0 should be conducted. In all cases, experimental procedures should be thoroughly described and where possible, uncertainties should be estimated and propagated in the calculation of B and F, and shown as error bars on the isotherm.

Frequently the isotherms on the MIP and an equivalent NIP are compared, as in figure 2. It was shown above that consideration of the MIP and NIP isotherm explains why IF is dependent on the ratio of analyte to polymer. Batch binding experiments can also be applied to derive selectivity factors. The MIP is incubated together with the target analyte, and an equivalent experiment is set up with a competitor, under identical conditions. Measurement of the free concentrations of analyte, and of competitor, then allows calculation of the selectivity factor α via equation 6. Consideration of a wider range of data for a target analyte and a competitor, presented as binding isotherms as in figure 10, allows us to see why α also is dependent on $n_{analyte}$, and may increase for lower ratios of $n_{analyte}$ to M_{MIP}

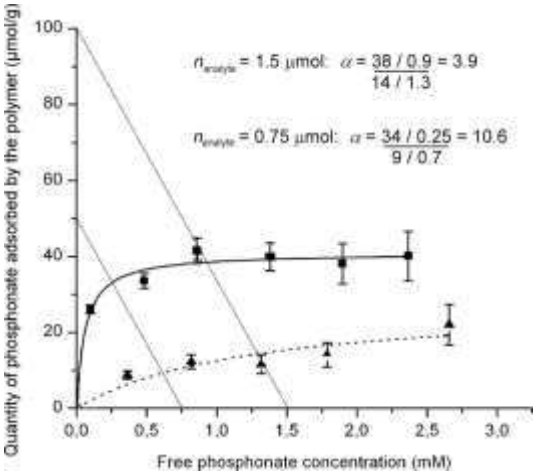

Fig. 10. An example of how distribution ratio (D) and selectivity factor (α) are influenced by ligand concentration. Data are for pinacolyl methylphosphonate (PMP, squares) and diphenylphosphinic acid (DPPA, triangles), incubated in 1 mL of toluene with 15 mg of PMP-imprinted MAA-co-DVB. Lines of ligand conservation drawn for $n_{analyte}$ = 1.5 µmol and 0.75 µmol. For the higher $n_{analyte}$, D_{PMP} = 42 mL g^{-1} and α = 3.9, while for the lower $n_{analyte}$, D_{PMP} = 136 mL g^{-1} and α = 10.6. Figure adapted with permission from [47].

Batch binding experiments can finally be applied to derive kinetic parameters. The MIP is incubated together with the target analyte, and after a specified time period the polymer is separated, the free analyte concentration F is measured and the bound concentration B calculated using equation 13. This procedure is repeated at different time intervals, allowing a curve to be drawn as in figure 11.

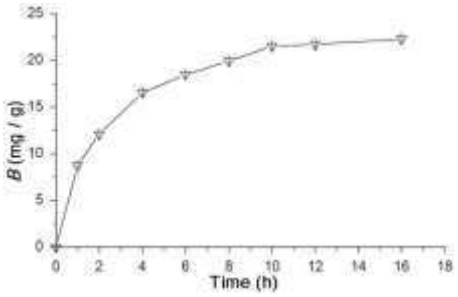

Fig. 11. Kinetic batch rebinding of hemoglobin (0.4 mg ml^{-1}) on hemoglobin-imprinted chitosan beads (0.5 g in 25ml buffer). Concentration determined after sedimentation of beads by absorbance at 280 nm. Figure reproduced with permission from [41].

The example in figure 11 is of extremely slow rebinding kinetics – attributable to the large size of the template (hemoglobin) which has been imprinted within large polymer particles. In contrast, kinetic batch binding studies of a small molecule binding to a MIP can show much faster kinetics (e.g. for chloramphenicol binding to a chloramphenicol-imprinted diethylaminoethylmethacrylate-co-EDMA polymer particles in THF, binding was observed to be essentially complete within 2 min [38]).

3b. Radioligand binding studies

A variation on the batch binding assay is where, rather than incubating polymer and analyte in the assay solvent, a mixture of polymer, analyte and radiolabelled probe are incubated in the assay solvent. When the radiolabelled probe is simply an isotopic variant of the analyte, it may be assumed that the probe binding directly reflects the analyte binding (equation 17, where $n_{\text{free probe}}$ is the amount of free radiolabelled probe in mol, and n_{probe} is the total amount of radiolabelled probe in the assay, in mol).

$$\frac{n_{\text{free}}}{n_{\text{analyte}}} = \frac{n_{\text{free probe}}}{n_{\text{probe}}} \tag{17}$$

$n_{\text{free probe}}$ can be measured, after separation of the solution from the polymer, by scintillation counting, and n_{probe} can be quantified by a control with no polymer. Thereafter equations 3 and 4 are used to derive B and F: the amount of probe is considered to be insignificant such that the total amount of analyte, n_{analyte}, is just equal to the unlabeled amount. An advantage of this approach is that it is adaptable to a huge range of (unlabelled) analyte concentration: since n_{probe} is the same in every assay the measurement of $n_{\text{free probe}}$ should not fall outside the instruments linear range even as n_{analyte} is varied over 5 or more orders of magnitude. Binding

assays have been performed in this way by the Mosbach group [26,25,48] and others [49] and data obtained in this way are shown in figures 4, 6, 7 and 9. It must be stressed that this approach assumes the absence of any isotopic fractionation i.e. the radiolabelled probe is assumed to bind in exactly the same way as the unlabeled analyte. If this condition is broken, equation 17 does not hold.

Selectivity can also be demonstrated using radioligand binding studies, where a mixture of polymer, analyte and radiolabelled probe in the assay solvent is compared with a mixture of polymer, competitor and radiolabelled probe. The ability of the analyte to displace the probe is compared with that of the competitor. The results may be plotted as $n_{\text{bound probe}}$ vs. $[\text{ligand}]_{\text{total}}$ where $[\text{ligand}]_{\text{total}}$ is the initial, added concentration (not the free concentration) of either the target analyte or the competitor. This is the principle of the competitive binding assay, or molecular imprint sorbent assay (MIA) first demonstrated for MIPs in a seminal Nature paper by Mosbach *et al*. in 1993 [25]. For best results, n_{probe} is chosen to be as low as possible (subject to the need for the proportion free in solution to be measured accurately by scintillation counting), the solvent and amount of imprinted material are then chosen such that when there is no additional target analyte or competitor, $n_{\text{bound probe}} / n_{\text{probe}}$ is in the range 0.5 to 0.8. Results for caffeine and theophylline binding to a caffeine-imprinted polymer are shown in figure 12.

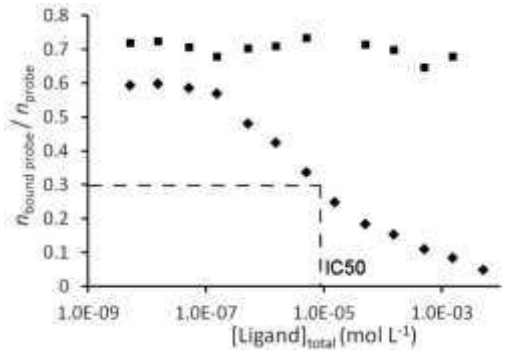

Fig. 12. Data for a MIA measuring the displacement of ^{14}C-caffeine probe from a caffeine-imprinted MIP by non-labelled caffeine (diamonds) and by theophylline (squares) [23]. Assays performed in 1 mL volume of heptane/THF (3:1 v/v) using 8 mg of MIP and varying amounts of unlabelled caffeine / theophylline.

The increased displacement of the probe from the MIP as the total concentration of target analyte is increased may be understood in terms of the binding isotherm for caffeine on this polymer as shown in figure 6. At very low concentrations, the distribution ratio *B/F* takes a relatively high value (e.g. 0.004 nmol mg^{-1} / 0.02 μM = 0.2 mL mg^{-1}, from which it may be calculated $n_{\text{bound}} / n_{\text{analyte}} \sim 0.6$, in agreement with figure 12). At high concentrations *B/F* takes a lower value, due to the curvature of the isotherm data (e.g. 30 nmol mg^{-1} / 5000 μM = 0.006 mL mg^{-1}, from which it may be calculated $n_{\text{bound}} / n_{\text{analyte}} \sim 0.04$, also in agreement). At about F = 10 μM, the experimental data suggest a B value of ~ 0.5 nmol mg^{-1}, giving

B/F = 0.05 mL mg^{-1}, from which it may be calculated n_{bound} / n_{analyte} ~ 0.3. The intermediate value where $n_{\text{bound probe}}$ / n_{probe} is exactly half the value it was in the absence of any non-labelled analyte, is known as the IC50. The relationship between the adsorption isotherm and the radioligand competition displacement curve is further discussed by Pap and Horvai [16].

Comparison of IC50 values for the target analyte and a particular competitor provides evidence for selectivity: if the sites which bind the probe are selective, then a competitor should be less effective at displacing the probe than the target analyte, and have a higher IC50. From figure 6 it may be seen that for this polymer, the IC50 for theophylline is in excess of 3mM and using equation 18 the MIA cross-reactivity is consequently ~ 0.3%. However, while the IC50 for the analyte can be related to the isotherm, as outlined above, there is no such simple relationship between the isotherm for the competitor and the IC50 value of the competitor, and the MIA cross-reactivity cannot readily be related to the selectivity of a batch binding experiment as described in equation 6.

$$\text{MIA cross} - \text{reactivity} = \frac{\text{IC50}_{\text{analyte}}}{\text{IC50}_{\text{competitor}}} \times 100\% \tag{18}$$

3c. Zonal chromatography

In many works, imprinted materials have been characterized by packing them into chromatography columns and measuring the retention times (t_R) of the analyte, and of competitors, when these are injected into a mobile phase flowing through the column. If the analyte exhibits a longer t_R than the competitor, this provides evidence for selectivity. This approach has been particularly used to demonstrate the separation of chiral mixtures, where one of the two enantiomers has been used as the template compound to generate an imprinted chiral stationary phase [50].

In conventional zonal chromatography under ideal, linear conditions, the retention time for an analyte should be related to its distribution ratio via equations 19-20:

$$k'_{\text{analyte}} = \frac{t'_{\text{R, analyte}}}{t_0} = \frac{t_{\text{R, analyte}} - t_0}{t_0} \tag{19}$$

and

$$k'_{\text{analyte}} = D\frac{M_{\text{stationary phase}}}{V_{\text{mobile phase}}} \tag{20}$$

where t_0 is the void time (the retention time for a non-retained species), $t'_{\text{R, analyte}}$ is the corrected retention time (=t_R - t_0), k'_{analyte} is the capacity factor, $M_{\text{stationary phase}}$ is the mass of stationary phase (e.g. MIP or NIP, in g) and $V_{\text{mobile phase}}$ is the vol-

ume of mobile phase (in mL). In theory, then, measurement of t_R enables calculation of D.

This simple model has been extended by various authors to consider the effects of the concentration of a modifier(/strong eluent) in the (weak) eluent on k'_{analyte}, and, hence, to propose the stoichiometry and affinity of the modifier-analyte, analyte-binding site and modifier-binding site interactions [51-53].

If t_R is measured for a competitor then

$$\alpha = \frac{D_{\text{analyte}}}{D_{\text{competitor}}} = \frac{k\prime_{\text{analyte}}}{k\prime_{\text{R, competitor}}} = \frac{t\prime_{\text{R, analyte}}}{t\prime_{\text{R, competitor}}} \tag{21}$$

In this way, selectivity factors are frequently calculated for the separation of peaks due to the imprinted, and non-imprinted enantiomers on an imprinted chiral stationary phase (Figure 13). However, this approach (like those in the previous paragraph) is based on the assumption that D is independent of the total amount of analyte injected, i.e. that the isotherm is linear, whereas in practice the isotherm is curved, so that D falls as the total amount of analyte increases (this can be seen from the chromatograms for increasing concentration of analyte in figure 14). Again, the highest values for α will usually be calculated when the ratio n_{analyte} / M_{MIP} is as small as possible i.e. when the lowest detectable amounts of analyte and competitor are injected onto the column (and when both the imprinted, and non-imprinted enantiomers will have longer retention times).

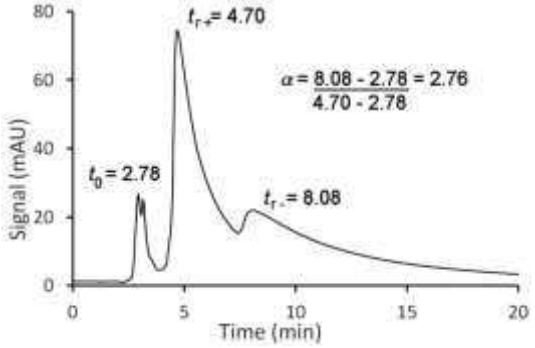

Fig. 13. Separation of enantiomers of ephedrine by zonal chromatography on an MIP stationary phase. (-)-ephedrine imprinted MAA-EDMA copolymer packed into 250 x 4.6 mm column. 200 μg (+/-)-ephedrine injected, chromatogram recorded at 254 nm using mobile phase of 20% AcOH in DCM, at 1.0 mL min^{-1} and 30º C[54].

Three measures of the quality of a chromatographic separation which are commonly encountered are the plate number N (which describes the sharpness of a peak), the asymmetry A_s (which describes the tailing or fronting of a peak) and the resolution R_s (which is a ratio of the separation of two peaks over their width). In the ideal case, N and R_s are independent of the amount of analyte loaded, and A_s = 1.0. When these parameters are compared, MIPs usually appear inferior to conventional stationary phases such as octadecylsilica.

The extreme tailing of the peaks often observed for zonal chromatography of analytes on MIPs (in particular, for the imprinted molecule itself) is attributed to the inhomogeneity of the binding sites and to slow binding/unbinding kinetics (the shape of the peaks can usually be improved by increasing the temperature of the column, which makes the rates faster) [55]. In figure 14, one can imagine the peak for 10 μg of analyte representing the binding to the strongest binding sites on the polymer: when 20 μg are injected there is too much anayte for the strongest binding sites, such that weaker sites are occupied too, giving a 'front' to the 10 μg peak. Likewise, one can picture the peak for 40 μg of analyte building on the front of the 20 μg peak, that for 100 μg of analyte building on the front of the 40 μg peak etc., as the extra analyte may only be retained by occupying weaker and weaker sites.

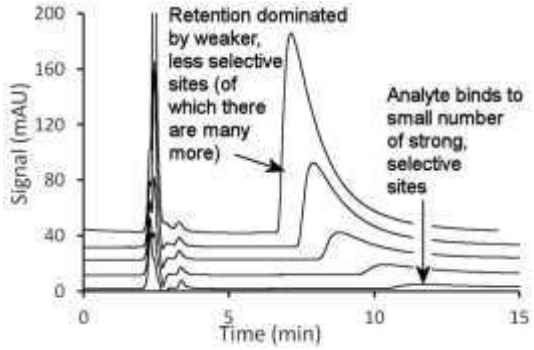

Fig. 14. Typical effect of increasing the amount of analyte injected on an MIP stationary phase in HPLC. MIP column is the same as for figure 13, chromatograms recorded at 254 nm using mobile phase of 5% $BuNH_2$ in DCM, at 1.0 mL min^{-1} and 30º C. Injections of increasing amounts of (-)-ephedrine: 10 μg (bottom), 20 μg, 40 μg, 100 μg, 200 μg (top). Peak at ~ 3 min is the void peak due to the solvent in which analyte is injected[54].

More sophisticated models of chromatographic behavior incorporating non-ideality and/or non-linearity begin with the general rate model, in which the mass balance for an analyte at distance z along the column and time t after injection is given by:

$$\frac{\partial C}{\partial t} + \frac{u}{\varepsilon}\frac{\partial C}{\delta z} + \frac{(1-\varepsilon)}{\varepsilon}\frac{\delta C_p}{\delta t} = D_L \frac{\delta^2 C}{\delta z^2} \qquad (22)$$

where C is the analyte concentration in the mobile phase (c.f. F, mol L^{-1}), u is the linear flow rate (cm s^{-1}), ε is the porosity as a fraction of the column volume, C_p is the analyte concentration in the pores (such that $\varepsilon \times$ total volume $\times C_p = M \times B$) and D_L is the dispersion coefficient ($cm^2 s^{-1}$), which is due largely to axial diffusion. This equation cannot be solved analytically, but with various additional assumptions, non-ideal and non-linear behavior can be modelled and various different predictions can be derived. Thus, Guiochon *et al*. have used a model derived from equation 22, together with binding isotherms derived separately by frontal

chromatography, to fit the peak shapes for (large volume and large concentration) injections of Fmoc-Trp enantiomers on an Fmoc-L-imprinted MIP, and derived kinetic parameters [56-60]. Horvai *et al*. have shown that if ideal behavior (neglecting kinetic effects) is assumed, points on the trailing edge of a peak such as that in figure 14 can be related to points on the isotherm [18,61] (the 'elution by characteristic point' method). Seebach and Seidel-Morgenstern used a similar relationship between the retention times for the peak maxima at a series of injected concentrations and B/F to derive an isotherm for Z-L-Phe binding to a Z-L-Phe MIP [62]. Baggiani *et al*. used a model derived from equation 22 but assuming a Langmuir-type isotherm to fit the complete peak shape for injections of pyrimethanil on pyrimethanil-imprinted MIPs, deriving apparent site densities and affinity constants as well as kinetic parameters [63]. Lee *et al*. have modelled the effect of sample concentration and affinity constant on the plate number and peak asymmetry [64].

3d. Frontal chromatography

In simple ('rectangular pulse') frontal chromatography, instead of injecting a short pulse of analyte, the mobile phase is altered to contain a specific concentration of analyte, which is run continuously through the column [65-67]. Initially, as it first enters the column, the analyte binds to binding sites on the stationary phase, however once the bound concentration of analyte reaches equilibrium with the concentration in the mobile phase over the whole of the column (as may be expressed via the distribution ratio for the analyte under those conditions) no more analyte can bind, and the analyte begins to elute from the column, the concentration in the eluent soon becoming the same as in the mobile phase which continues to be fed on to the column. The measured parameter is the breakthrough time, $t_{\text{breakthrough}}$ (or, frequently, the breakthrough volume, V_r in mL, which is just $t_{\text{breakthrough}}$ × the volumetric flow rate (f, L min^{-1})), which is the interval from the point at which the mobile phase is changed, to the time when the analyte appears in the eluent.

The amount of analyte bound to the stationary phase is given by:

$$n_{\text{bound}} = f \times \left(t_{\text{breakthrough}} - t_0\right) \times [A] \tag{23}$$

where t_0 is the void time as before (and will correspond to $t_{\text{breakthrough}}$ if none of the analyte at all was to bind to the stationary phase), and $[A]$ is the concentration (mol L^{-1}) of analyte added to the mobile phase. The distribution ratio (equation 3) is given by:

$$D = \frac{B}{F} = \frac{f \times \left(t_{\text{breakthrough}} - t_0\right)}{M_{\text{MIP}}} \tag{24}$$

and hence the binding isotherm can be derived. Data obtained in this way can readily be fitted to a model assuming all binding sites are equivalent (i.e. a Langmuir model). If this is the case, the total number of binding sites n_{total} is given by $n_{\text{total}} = n_{\text{empty}} + n_{\text{bound}}$ and (from equation 2)

$$K_{\text{d}} = \frac{n_{\text{empty}} \times F}{n_{\text{bound}}} = \frac{n_{\text{total}} \times F}{n_{\text{bound}}} - F \tag{25}$$

substituting F=[A] and for n_{bound} as in equation 23 gives

$$K_{\text{d}} = \frac{n_{\text{total}}}{f \times (t_{\text{breakthrough}} - t_0)} - [A] \tag{26}$$

Thus, a series of experiments are performed applying different concentrations of analyte in the mobile phase. $t_{\text{breakthrough}}$ is measured, then the column regenerated to remove all bound analyte and the experiment repeated using a different concentration. A plot of $1/([A] \times f \times (t_{\text{breakthrough}} - t_0))$ against $1/[A]$ should give a straight line with y-intercept $1/n_{\text{total}}$ and x-intercept $-1/K_{\text{d}}$.

Mosbach *et al*. were first to apply this approach to MIPs, deriving apparent n_{total} values in the range 18-28 μmol g^{-1} of polymer, K_{d}s in the range 1.6 to 8.1 mM, and showing that MIPs had lower K_{d} values (indicating stronger binding) for their template than its optical antipode, and lower K_{d}s than the corresponding NIPs, as expected [68,69]. Andersson *et al*. applied frontal chromatography to a model system of pyridines and bipyridines binding to 4,4'-bipyridyl-imprinted MAA-co-EDMA in order to demonstrate the increased strength of binding when more than one analyte-monomer interaction is present within the imprinted site [70]. The approach has also been used extensively by Baggiani *et al*.[71,72] and others [73,74]. In one intriguing study, Baggiani *et al*. compared the rebinding of 2,4,5-trichlorophenoxyacetic acid (2,4,5-T) to a conventional 2,4,5-T-imprinted 4-vinylpyridine-co-EDMA polymer and a polymer which, additionally, incorporated a covalently bound template analogue, and showed that the latter polymer had a lower binding capacity (lower n_{total}) but lower K_{d} (i.e., the covalently incorporated template analogue appeared to increase the strength of template re-binding)[3].

A variant of frontal chromatography is staircase frontal chromatography, in which, once the detector signal has stabilized showing that the analyte is present in the eluent at the same concentration as in the injected mobile phase, the mobile phase is altered to contain a higher concentration of the analyte, and the process repeated giving a chromatogram with the appearance of a staircase, indicating a series of concentration steps. This approach was first applied to MIPs by Guiochon *et al*. [29]. On proceeding from step i to step i+1, the additional amount of analyte bound to the stationary phase can be calculated as :

$$n_{\text{bound},\, i+1} - n_{\text{bound},\, i} = f \times \left(t_{\text{breakthrough}} - t_0\right) \times \left([A]_{\,i+1} - [A]_i\right) \tag{27}$$

from which the isotherm can be derived in shorter time than would be required by the rectangular pulse method (where the column must be regenerated between each change in concentration). Figure 15 shows typical data.

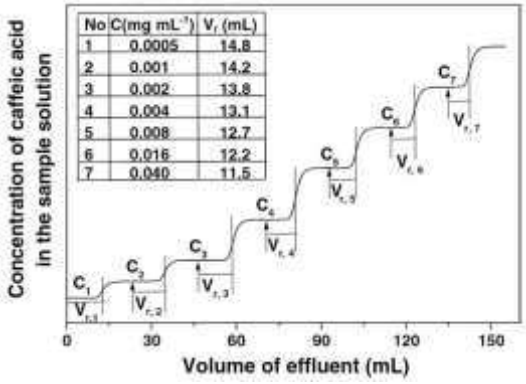

Fig. 15. Partial frontal chromatogram of caffeic acid on caffeic acid-imprinted MAA-co-EDMA monolith in a 200 x 4.6 mm column with THF mobile phase at 25 ºC and 0.5 mL min^{-1}, monitored at 280 nm. Arrows mark introduction of sample solutions having the concentration indicated. Reproduced with permission from [28].

The shape of the 'front' or breakthrough curve can also give information about the shape of the isotherm, as well as the kinetics of analyte binding to the stationary phase. For example, figure 16 shows a typical breakthrough curve obtained by Guiochon *et al*. $t_{\text{breakthrough}}$ is the time corresponding to half-height of the front, i.e. the centre of mass of the concentration step, in this case 6.75 min. A classical transport model was applied to model the breakthrough curve, involving numerical solutions of an equation derived from equation 22. The modelled curves require as an input a relationship between B and F for any particular F at equilibrium (i.e. a theoretical isotherm, see section 2), and an estimated value for the mass transfer rate coefficient k_f (in min^{-1}), which is related to, though not identical to, the forwards rate constant k_1 in equations 7 and 8, and defined as:

$$\frac{\partial B}{\partial t} = k_{\text{f}}(B_{\text{eqm}} - B_t) \tag{28}$$

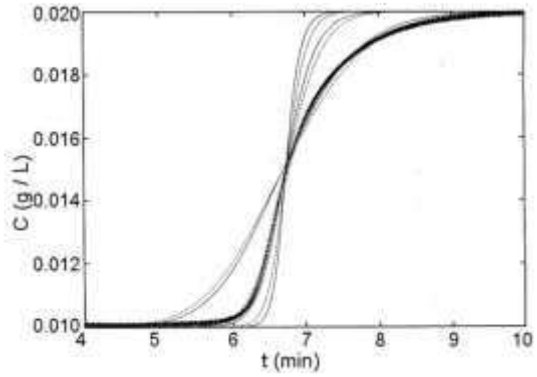

Fig. 16. Experimental breakthrough curve (symbols) and fitted curves (lines) for L-Phe-An applied to a L-Phe-An imprinted MAA-co-EDMA polymer, packed into a 100 x 4.6 mm column. Mobile phase of MeCN-0.05 M potassium phosphate (7:3 v/v) at 1.0 mL min^{-1} and 40°C, monitored at 260 nm. The concentration step shown is from C_n=0.01 to C_{n+1}=0.02 g/l. Calculated breakthrough curves for k_f=10 min^{-1}, k_f=110 min^{-1} and for the rate coefficient which fits best the experimental data, k_f=40 min^{-1} (the larger k_f, the steeper the curve). Solid lines: Bi-Langmuir model. Dashed lines: Freundlich model. Reproduced with permission from [29].

For the concentration step shown in figure 16, the classical transport model provides the best fit to the data when the isotherm is considered to be of the bis-Langmuir form and k_f is given the value 40 min^{-1}. For a sequence of concentration steps, k_f was found to increase with an increase in [A], to increase with temperature, and to be lower for the imprinted enantiomer than its optical antipode (particularly at lower concentrations). The latter effect may be rationalized by the strongest, most selective binding sites being also the less accessible, hence slower binding ones [29]. The values of k_f found are low in comparison with other types of stationary phase, supporting the thesis that slow mass transfer contributes to the poor peak shapes seen in zonal chromatography, as well as binding site heterogeneity.

Staircase frontal chromatography was used further, in combination with models of non-ideal, non-linear chromatographic behavior, in a series of works by Guiochon *et al*. to show the effects of heat-treating the MIP [75,76], the effects of the pH [77] and temperature [60] of the mobile phase, the effects of different organic mobile phases [78], of organic modifiers added to an acetonitrile mobile phase [79,80], and of water in an organic-aqueous cosolvent mobile phase [58], to compare particulate and monolithic MIP stationary phases [81], to compare the retention of template analogues [82] and to deconvolute the effects of different kinetic processes in the lumped mass transfer rate coefficient k_f: it was shown that in some cases diffusion within the pores of the MIP particles makes the largest contribution to the slow rate constants [83], and in other cases surface diffusion [56,57].

3e. Calorimetry

When the target analyte (or a competitor) binds to an imprinted binding site, there is expected to be a change in enthalpy *H*. If the binding process is thermodynamically favorable then the change in Gibbs free energy, ΔG for the process must be negative, where ΔG is related to the changes in enthalpy and entropy, *S*:

$$\Delta G = \Delta H - T \times \Delta S \tag{29}$$

Hence a spontaneous (exergonic) process can be driven by a negative ΔH (exothermic) or by a positive ΔS (increase in entropy). Bond formation is usually exothermic.

Isothermal titration calorimetry (ITC) was first applied to imprinted materials by Chen *et al*. [84] and has subsequently been used by others [85-90], while batch calorimetry has also been used to study slow binding processes [88,91,92]. In batch calorimetry, two solutions are allowed to reach thermal equilibrium separately within the calorimeter, then mixed and the heat produced *Q* is measured over time. ITC is similar except that one solution, the titrant, is added via automated syringe in very small aliquots to the other, which is in a cell in the calorimeter. The heat is measured as the power (W, Js^{-1}) which is produced / taken in by the cell as a function of time, producing a spike on each injection (e.g. figure 17A) which can be integrated and divided by the amount of titrant added to give a decaying profile such as figure 17B.

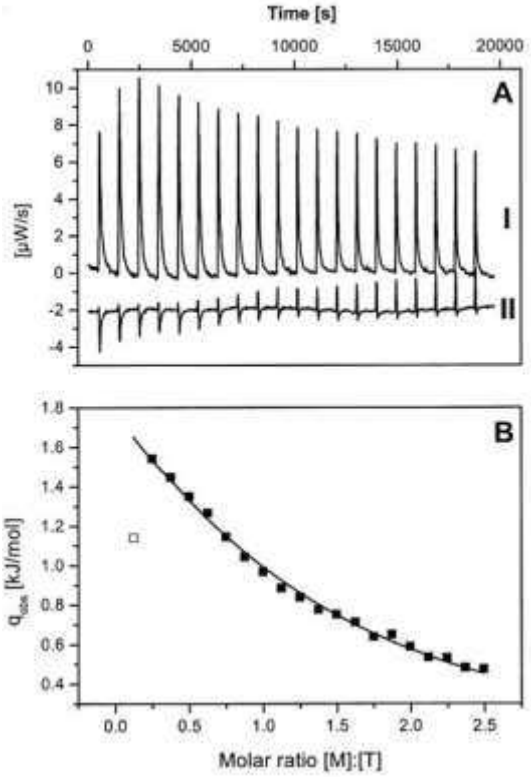

Fig. 17. (A) Experimental titration curves for the titration of Boc-L-Phe-An imprinted and -extracted microgel A at 25ºC (I) and the corresponding control dilution experiment (II). Measured heat power vs. time. A suspension of microgel in methanol/water (50:50 v/v) was titrated into Boc-L-Phe-An dissolved in the same solvent. (B) Observed titration heat Q_{step} versus molar ratio microgel to template (the first value was excluded from analysis). Reproduced with permission from [90].

The sample in the cell might be the imprinted material, with the target analyte added from the syringe, but in the experiment shown in Figure 17 the set-up was with the target analyte (Boc-Phe-An) in the cell and a suspension of imprinted nanoparticles in the syringe [90]. When the adsorption isotherm has been obtained independently, it may be possible to know exactly how much analyte binds to the imprinted polymer in each step ($n_{\text{bound after step}} - n_{\text{bound before step}}$), in which case:

$$Q_{\text{step}} = \Delta H \times \left(n_{\text{bound after step}} - n_{\text{bound before step}}\right) \tag{30}$$

If the binding isotherm is not known, the data can be converted to display $Q_{\text{cumulative}}$ against $[\text{titrant}]_{\text{total}}$ and fitted with a function assuming a single class of identical binding sites, derived from equation 31-32:

$$Q_{\text{cumulative}} = \Delta H \times n_{\text{bound cumulative}} \quad (31)$$

$$n_{\text{bound}} = K_a \times (n_{\text{total}} - n_{\text{bound}}) \times ([\text{analyte}]_{\text{total}} - n_{\text{bound}} \times M/V) \quad (32)$$

where M and V have their usual meaning. This yields n_{bound} as the root of a quadratic, and the function can be fit to yield ΔH, n_{total} and K_a (in the case of Weber *et al*. [90], n_{total} was estimated independently).

In these or equivalent ways, quite varying values of ΔH have been obtained: +8 kJmol^{-1} for 2,4-D binding to a imprinted VPy/EDMA polymer in aqueous buffer [84], +6.6 kJmol^{-1} for phenylmannopyranoside binding to a vinylphenylboronic acid/EDMA polymer in acetonitrile [88], -21 kJmol^{-1} for Boc-L-Phe-An binding to the polymer shown in figure 17 [90], -8 kJ kJmol^{-1} for riboflavin binding to a 2,6-bis(acylamido)pyridine polymer in water/ethanol/formic acid (90.6:4.7:4.7 v/v/v).

In some cases, the further extension has been made that, if the conditions can be approximated to standard conditions,

$$\Delta H = \Delta H^{\theta} = \Delta G^{\theta} + T \times \Delta S^{\theta} \quad (29)$$

and since

$$\Delta G^{\theta} = -RT \ln K_a \quad (30)$$

the entropy change on binding, S may also be estimated. There seem to be rather too many assumptions underlying quantitative estimates like this: however it may certainly be said that if the process is observed to be endothermic, as in Chen *et al*.s study of 2,4-D binding to a imprinted VPy/EDMA polymer in aqueous buffer [84], then the binding must be driven instead by an increase in entropy. This makes sense in the case of binding in water, where hydrophobic interactions are well-known to be entropically driven.

3f. Other methods

Since the application envisaged for many MIPs is in solid-phase extraction/sample clean-up of a dilute analyte in a complex matrix prior to quantitative analysis by HPLC, LC-MS or GC, Martin-Esteban *et al*. have attempted to derive isotherms for analytes binding to MIPs under SPE-type conditions [35,36,93]. In an experiment which is similar to a batch-binding experiment, analyte in binding solvent (1 mL, 0.05 – 500 mg L^{-1}) was loaded onto pre-conditioned MIP (100 mg) packed into a SPE cartridge. Some, but not all, the analyte bound under these conditions. A washing solvent was applied, followed by the elution solvent (3-8 mL). The eluted fraction was concentrated, and analysed by HPLC to determine n_{bound}. n_{free} was calculated as the difference between the amount loaded, n_{analyte}, and n_{bound}.

Data were then fitted using Langnuir-Freundlich isotherms. Although the approach was certainly useful in characterizing MIPs for SPE, the validity of the isotherm fits is questionable because binding did not necessarily occur under equilibrium conditions, and there is no way of assessing the effect of kinetic limitations.

Spectroscopic interrogation of an MIP, in its clean state and after binding of analyte, forms the basis of many proposed applications of MIPs in chemical sensing. However, such an approach can also provide useful information about the nature of analyte-binding site interactions, including some indication of their strength. Hsu *et al*. used infrared (IR) spectroscopy to monitor the binding of thymine to thymine-imprinted diacryloyl-2,6-diaminopyridine-co-tripropyleneglcol diacrylate polymer films in chloroform [94]. Distinctive absorbances were observed due to the bound and non-bound thymine: by assuming the measured absorbances to be proportional to B and to F, apparent binding constants K_a' could be calculated. Resmini *et al*. used a similar approach based on the quenching of the visible absorbance (435 nm) of a phosphate template when it rebinds to an arginine-containing MIP in DMSO, to calculate the binding site population (assuming a stoichiometric rebinding) [95]. Haupt *et al*. used the Raman signal produced when propranolol was added to a propranolol-imprinted MIP and a NIP in MeCN to plot a form of isotherm and calculate apparent binding constants K_a' (their approach assumes the free propranolol concentration is identical to the added concentration) [96]. In each of these examples, the sensor response (change in absorbance of the polymer) is assumed to be proportional to B (or n_{bound}). This assumption was tested for two MIP systems by Ng and Narayanaswamy [97]. Cu^{2+} binding to copper-imprinted 4-vinylpyridine-co-hydroxyethylmethacrylate-co-EDMA polymer particles in water was measured both by batch binding (supernatant added to eriochrome cyanine R and absorbance recorded at 568 nm) and by reflectance measurements at 750 nm on a layer of particles deposited on the tip of a fibre-optic bundle. *N*-phenyl-1-naphthylamine (NPN) binding to NPN-imprinted 2,4-diisocyanate cross-linked β-cyclodextrin particles in methanol was measured by batch binding (direct measurement of supernatant absorbance at 340 nm) and fluorescence measurements (λ_{ex} = 365 nm, λ_{em} = 495 nm) on particles trapped in a fluorescence flow cell. The authors suggest a good correlation in each case, although a simple comparison of signal and B for differing F is not presented: more studies of this kind are needed in order to correlate sensor signals with binding isotherms.

Apparent isotherms can be recorded, and apparent affinity constants calculated, using other sensor techniques such as surface plasmon resonance [98] and quartz crystal microbalance [99,100]. Such analyses again rely on the assumption that the sensor response is proportional to B (or n_{bound}).

Another experimental measurement of analyte-MIP interactions which has been proposed is force measurements using AFM. In the first example of such work by Haupt *et al*., the binding of cytochrome-C (immobilized on an AFM tip) to protein-imprinted acrylamide-co-bisacrylamide hydrogel films covalently coupled to glass slides was measured by force measurements. The interaction with imprinted films was stronger than with non-imprinted, and was correlated with the

binding of fluorescein-labelled cytochrome-C from aqueous buffer [101]. Recent work by Reddy *et al*. [102], yielded similar data for the binding of bovine hemoglobin (immobilized on an AFM tip) to protein-imprinted hydrogel particles.

In parallel with experimental studies, the interactions of analytes with MIPs have been modelled *in silico* [103]. Although there are less examples of computational studies on MIPs than on the pre-polymerization mixture (reflecting the greater complexity of the polymerized material), this is a field of increasing activity.

4. Parameters influencing rebinding

4a. Polymer design

MIP design cannot be dealt with in this chapter, but it should be emphasized that the binding properties of a MIP (and NIP) are inextricable from its composition and method of preparation. The major factors influencing the binding properties of the resulting polymer include the type of functional monomer and monomer:template ratio [1,9,104-106] and the porogenic solvent [105,107].

4b. Rebinding solvent (organic solvents)

For MIPs prepared via non-covalent imprinting using hydrogen-bonding interactions (e.g., the vast majority of MIPs produced used MAA as functional monomer), a non-polar organic solvent is commonly used as porogen (to promote the monomer-template interactions), and the strongest and most selective rebinding is also often observed in a non-polar organic solvent. Dogma suggests that, for this class of MIPs, the rebinding will be strongest and most selective in the same solvent which was used as the porogen (because the swelling of the MIP is assumed to be different in different solvents, affecting the binding site integrity). This is frequently the case (e.g. 4-nitrophenol-imprinted 4-vinylpyridine-co-DVB particles gave the best separation between 4-nitrophenol and its isomers in zonal chromatography using a chloroform mobile phase if the porogen was chloroform, and using an MeCN mobile phase if the porogen was MeCN [107]), but not always (2-(morpholin-4-yl)ethyl (2-methoxyphenyl)carbamate-imprinted MAA-co-EDMA particles made with toluene porogen gave stronger binding of the template and its isomers in zonal chromatography using a toluene mobile phase than using MeOH, but the separation factors and *IF*s were higher using MeOH than using toluene [108]). Guiochon *et al*. obtained isotherms for Fmoc-L-Trp on a Fmoc-L-Trp-imprinted 4-VPy-co-EDMA particles using staircase frontal analysis: the MIP was

made with MeCN as porogen and exhibited higher affinity and selectivity for the template in MeCN than in DCM, chloroform, or THF. The isotherm in MeCN was well-fitted to a tri-Langmuir model, but in the other solvents a bi-Langmuir model fitted best suggesting that the strongest adsorbing sites were absent [78]. The influence of solvent dielectric constant and Snyder polarity index on rebinding of bupivacaine to a bupivacaine-imprinted MAA-co-EDMA in single-point experiments has been studied by Rosengren *et al*. [109].

Commonly a polar organic modifier is added to the organic solvent in which analyte binding to a MIP is being studied – the modifier serves to reduce the strength of binding. This is often desirable so as to promote selective binding, rather than non-selective i.e. the modifier is thought to reduce binding to the weak, non-selective hydrogen bonding sites of the polymer more than it reduces binding to the strong, selective sites [9]. In MIA binding assays, in SPE, and in the use of MIPs as stationary phases in chromatography, the effect of increasing amounts of modifier on binding to the MIP and NIP is often compared, to find the modifier concentration at which the *IF* is maximized. The influence of type and concentration of modifiers on the binding of Fmoc-L-Trp to Fmoc-L-Trp-imprinted 4-VPy-co-EDMA particles was also studied in detail by Guiochon *et al*. using staircase frontal analysis. Isotherms were obtained and fitted to tri- or tetra-Langmuir models. Modifiers were found to reduce the density, B_{max} of the strongest binding sites more than the K_a, but reduce the K_a of the weak binding sites more than their B_{max} [79,80].

4c. Rebinding pH and cosolvent (aqueous)

MIPs dependent on weak hydrogen bonds between the template and binding site do certainly work best in organic solvents, and furthermore the sugar-imprinted polymers studied by Wulff in the 1970s and 1980s (based on the covalent interactions between sugars and boronic acids) had a similar preference. This led to a prejudice among the wider scientific community that MIPs could not work in aqueous solvents. Nowadays there are numerous examples of MIPs both made in, and applied in, aqueous buffers or aqueous / organic cosolvent mixtures. MAA- or 4-VPy-based polymers can show good binding and selectivity in aqueous buffers if the analyte-polymer interaction is strong [110,111].

Often for small molecules, an organic-aqueous cosolvent mixture is used. Pure aqueous conditions lead to significant hydrophobic interactions, which for MIPs made in organic solvents using DVB or EDMA as cross-linker, lead to significant non-specific adsorption of the analyte, outside of the more selective sites. A certain amount of organic cosolvent can minimize these non-specific interactions, but must usually be carefully optimized e.g. Dong *et al*. have optimized an organic-aqueous mobile phase for zonal chromatographic separation of the enantiomers of ephedrine on a (+)-ephedrine-imprinted MAA-co-EDMA polymer [112]. Furthermore, the pH of the aqueous phase is usually critical, when the analyte and/or

functional groups of the MIP are ionizable. Sellergren and Shea proposed a model for the influence of pH on retention and separation of the enantiomers of Phe-An on a Phe-L-An-imprinted MAA-co-EDMA polymer in zonal chromatography [113]. At pH 4 and below, both the analyte and the carboxylate groups of the MIP are protonated, the cationic analyte interacts only weakly with the neutral polymer. At pH 8 and above, both the analyte and the carboxylate groups of the MIP are deprotonated, the neutral analyte however interacts only weakly with the anionic polymer. In the intervening region, there is some overlap between the carboxylate groups being deprotonated and anionic and the analyte protonated and cationic – so binding is strongest. However, selectivity peaks at about pH6, which was proposed to correlate with the carboxylate functions of the strongest, most selective sites having a lower average pK_a than the weaker, non-selective sites.

Guiochon *et al*. have also studied the influence of the fraction and pH of aqueous cosolvent in an acetonitrile mobile phase on the isotherms for Phe-An [77] and Fmoc-Trp [58] enantiomers on their respective MIPs, obtained via staircase frontal analysis. In the former case, the isotherms supported the conclusions of Sellergren and Shea, with the number of weak binding sites increasing faster with pH than the number of strong binding sites. For Fmoc-Trp, the highest number of binding sites was calculated at pH3.8, where both the analyte and polymer (4-VPy based) are neutral: this corresponded to zonal chromatography where the highest retention was at this pH. Selective binding in this case appears to be driven more by hydrophobic interactions and hydrogen bonds, than by ion-pair formation.

4d. Temperature

The first detailed study of the effect of temperature on MIP binding properties was reported by Sellergren and Shea [55]. The binding of the enantiomers of Phe-An to an L-Phe-An-imprinted MAA-co-EDMA polymer was studied in zonal chromatography using an MeCN-aqueous buffer mobile phase and an MeCN-AcOH mobile phase at temperatures between 20 and 80 ºC. For the aqueous mobile phase, increasing temperature lead to a partial improvement in the peak shape (suggesting an acceleration of the kinetics), a decrease in the retention of both enantiomers (suggesting binding is an exothermic, enthalpy-driven process) and a decrease in separation (suggesting binding of the imprinted enantiomer is more exothermic than that of its optical antipode). For the organic mobile phase a partial improvement in the peak shape was again observed, but there was an increase in the retention of both enantiomers (suggesting binding is an endothermic, entropy-driven process) and an increase in separation.

Hsu *et al*. also studied the effect of temperature on the K_a' values obtained for thymine binding to their thymine-imprinted diacryloyl-2,6-diaminopyridine-cotripropyleneglcol diacrylate polymer films in chloroform, observed using IR as described in section 3f [94]. The apparent binding strength decreased with an in-

crease in temperature, and an exothermic ΔH and corresponding ΔS were calculated.

Guiochon *et al*. also studied the influence of the temperature on the isotherms for Fmoc-Trp enantiomers on the Fmoc-L-Trp-imprinted MIP, via staircase frontal analysis with an MeCN-AcOH (99:1 v/v) mobile phase [56,57,60]. ΔH, ΔS and kinetic parameters were calculated for the different classes of site that appeared to contribute to the isotherms fitted with bi- and tri-Langmuir models. Whilst it was concluded that binding overall was enthalpy-driven, the dominant driving force for transfer of the imprinted enantiomer to the strongest, most selective sites was proposed to be entropic.

5. Binding site affinity distributions

The number of binding sites and their binding affinities are parameters in the Langmuir, bi-, tri-and multi-Langmuir isotherms: hence when an isotherm is fitted using these models, a simplistic picture of the classes of sites (each class having a unique K_a and B_{max}) is immediately available. In reality, however, as explained in the introduction, there will not be distinct classes of binding sites but rather a continuum, from strong and selective sites present in small numbers to weaker and less selective sites present at far greater densities. Both the Freundlich and Langmuir-Freundlich isotherms allow for such a distribution of sites, and the number of sites B_i with a particular affinity constant K_{ai} can be calculated from the isotherm fitting and displayed as an *affinity distribution* (figure 18). These models are restrictive however, in that the shape of the distribution is fixed (for the Freundlich isotherm, it is an exponentially decaying distribution starting with an infinite number of binding sites with $K_a = 0$, for Langmuir-Freundlich, it is a gaussian distribution). An alternative approach involves converting the isotherm data directly to an affinity distribution without applying any fixed isotherm model: such an approach is valuable but depends on data of extremely high quality.

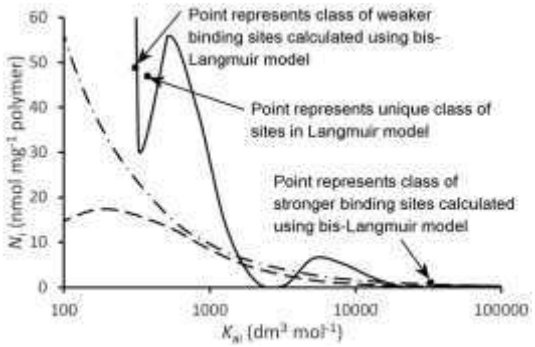

Fig. 18. Affinity distributions, calculated from *B*-*F* data for a caffeine-imprinted MIP as in figure 4 [23]. Curves for affinity distributions calculated using a numerical model without imposing an isotherm (solid line), or imposing Freundlich (dot-dash) and Langmuir-Freundlich (dashed) isotherms, all calculated and displayed using Microsoft Excel™. Step size $\ln K_{ai} - \ln K_{a(i-1)}$ for the Langmuir-Freundlich and numerical affinity spectra is 0.2.

Shimizu *et al*. were first to calculate an affinity distribution from binding data for a MIP[114]. The method is non-trivial. First, it is assumed that the concentration of bound ligand for a particular free ligand concentration is obtained by integration over all binding sites with differing affinities K_{ai} (equation 31):

$$B = \int_{-\infty}^{\infty} \frac{B_i \times F \times K_{ai}}{1 + K_{ai} \times F} d(\log K_{ai}) \tag{31}$$

This expression cannot be solved analytically for any particular set of *B* and *F* values. However, an approximate solution was developed by Hunston (equations 32-36):

$$B_i = \left| \frac{B_1 - B_2}{2 \log \alpha} - \frac{\alpha \times ((B_3 - B_4) - 2(B_1 - B_2))}{2(\alpha - 1)^2 \times \log \alpha} \right| \tag{32}$$

Equation 32 gives the density of binding sites for a particular value of K_{ai} where

$$B_1 = B \quad \text{at} \quad F = \frac{\alpha}{K_{ai}} \tag{33}$$

$$B_2 = B \quad \text{at} \quad F = \frac{1}{\alpha \times K_{ai}} \tag{34}$$

$$B_3 = B \quad \text{at} \quad F = \frac{\alpha^2}{K_{ai}} \tag{35}$$

$$B_4 = B \quad \text{at} \quad F = \frac{1}{\alpha^2 \times K_{ai}} \tag{36}$$

α is the step size (i.e. B_i is actually the density of binding sites with association constants in the interval B_i to $(B_i+\alpha)$). The values B_1 to B_4 must be interpolated from the calculated *B*-*F* data, and precise values are essential. To avoid imposing any model on the data, they are fitted using a smoothed spline. In this way, the values of B_i displayed in figure 18 are obtained. Note that the treatment only has any validity in the range $1/F_{max} \leq K_{ai} \leq 1/F_{min}$ where F_{max} and F_{min} are the highest and lowest values of *F* in the measured binding data. In this case, the numerical model interestingly produces a curve with two maxima, suggesting two broad site populations, which are not too different from the points corresponding to the two classes of binding site calculated from the bis-Langmuir model.

An alternative method for solving equation 31 to produce an experimental affinity distribution without imposing any model on the *B-F* data has been described by Guiochon *et al* [115].

More simply than the numerical methods, which make no assumptions of any particular isotherm, equation 31 can be solved analytically if a Freundlich isotherm is assumed [32], and whilst it cannot be solved analytically for the Langmuir-Freundlich isotherm, if *B-F* data are fitted to the Langmuir-Freundlich then the fitted parameters can be used to calculate B_1 to B_4 for differing values of K_{ai} in equations 33 to 36 above [34] and hence the affinity distribution can be derived. These methods were used to derive the curves in figure 18 and 19. Clearly the Freundlich isotherm gives rise to an exponentially decaying distribution, whilst the Langmuir-Freundlich isotherm gives rise to a Gaussian distribution with a clear maximum. Of course, neither model is really valid in the range $K_{ai} < 1/ F_{max}$ (in this case, $K_{ai} < 200$ M^{-1}, the region greyed out in figure 11) and both models are in reasonable agreement at higher K_{ai}.

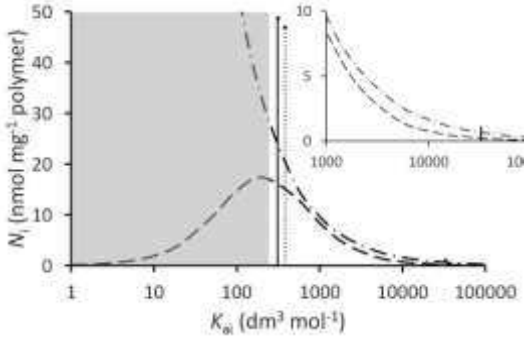

Fig. 19. Affinity distributions, calculated from *B-F* data for a caffeine-imprinted MIP as in figure 4 [23]. Curves for Freundlich (dot-dash) and Langmuir-Freundlich (dashed) isotherms calculated and displayed using Microsoft Excel™. Dotted line indicates the homogeneous binding site population predicted by the Langmuir isotherm, and solid lines the two homeogeneous populations predicted by the bi-Langmuir isotherm. Inset shows the values at high K_i, to emphasise the high-affinity sites in the bi-Langmuir approximation at ~30000 M^{-1}. Step size $\ln K_{ai} - \ln K_{a(i-1)}$ for the Langmuir-Freundlich isotherm is 0.2. The region where $K_{ai} < 1/ F_{min}$, for which the fits are not really valid, is greyed out.

Batch rebinding data have been fitted to the Freundlich isotherm and converted to affinity distributions by Mizaikoff *et al*. [116], Diaz-Garcia *et al*. [38] and others. The alternative methods to derive affinity distributions have been reviewed by Shimizu *et al*. [30].

6. Conclusions

The binding properties of molecularly imprinted polymers have been reviewed, with particular emphasis on the binding / adsorption isotherm and on the methods employed to characterize binding strength, selectivity and kinetics.

The defining characteristic of the binding sites in a MIP is heterogeneity, such that single-point measurements (i.e., studying binding using a unique concentration of analyte and amount of polymer) will always yield different values for the binding strength, selectivity and kinetics. Experimental capture of an isotherm is desirable, although it may not always be necessary if the MIP is being synthesized for a specific use and can easily be tested for efficacy in that application.

The detailed and extensive studies by Guiochon *et al*. have been exemplary in characterizing binding properties and their dependence on solvent composition and temperature. The simplistic model of one class of strong, selective sites and one of weak, non-selective sites has been shown to be a great simplification of the real situation, but remains a useful picture.

References

1. Andersson HS, Karlsson JG, Piletsky SA, Koch-Schmidt AC, Mosbach K, Nicholls IA (1999) Study of the nature of recognition in molecularly imprinted polymers, II 1 - Influence of monomer-template ratio and sample load on retention and selectivity. Journal of Chromatography A 848 (1-2):39-49. doi:10.1016/s0021-9673(99)00483-5

2. Katz A, Davis ME (1999) Investigations into the mechanisms of molecular recognition with imprinted polymers. Macromolecules 32 (12):4113-4121. doi:10.1021/ma981445z

3. Baggiani C, Giraudi G, Giovannoli C, Tozzi C, Anfossi L (2004) Adsorption isotherms of a molecular imprinted polymer prepared in the presence of a polymerisable template - Indirect evidence of the formation of template clusters in the binding site. Analytica Chimica Acta 504 (1):43-52. doi:10.1016/s0003-2670(03)00671-8

4. Lavignac N, Brain KR, Allender CJ (2006) Concentration dependent atrazine-atrazine complex formation promotes selectivity in atrazine imprinted polymers. Biosens Bioelectron 22 (1):138-144. doi:10.1016/j.bios.2006.03.017

5. Kim H, Spivak DA (2003) New insight into modeling non-covalently imprinted polymers. Journal of the American Chemical Society 125 (37):11269-11275. doi:10.1021/ja0361502

6. Kobayashi T, Fukaya T, Abe M, Fujii N (2002) Phase inversion molecular imprinting by using template copolymers for high substrate recognition. Langmuir 18 (7):2866-2872. doi:10.1021/la0106586

7. Yoshikawa M (2001) Molecularly imprinted polymeric membranes. Bioseparation 10 (6):277-286. doi:10.1023/a:1021537602663
8. Stahl M, Jeppssonwistrand U, Mansson MO, Mosbach K (1991) Induced stereoselectivity and substrate selectivity of bio-imprinted alpha-chymotrypsin in anhydrous organic media. Journal of the American Chemical Society 113 (24):9366-9368
9. Ansell RJ, Kuah KL (2005) Imprinted polymers for chiral resolution of (+/-)-ephedrine: understanding the pre-polymerisation equilibrium and the action of different mobile phase modifiers. Analyst 130 (2):179-187. doi:10.1039/b408751h
10. Benito-Pena E, Urraca JL, Sellergren B, Cruz Moreno-Bondi M (2008) Solid-phase extraction of fluoroquinolones from aqueous samples using a water-compatible stochiometrically imprinted polymer. Journal of Chromatography A 1208 (1-2):62-70. doi:10.1016/j.chroma.2008.08.109
11. Hall AJ, Manesiotis P, Emgenbroich M, Quaglia M, De Lorenzi E, Sellergren B (2005) Urea host monomers for stoichiometric molecular imprinting of oxyanions. Journal of Organic Chemistry 70 (5):1732-1736. doi:10.1021/jo048470p
12. Lubke C, Lubke M, Whitcombe MJ, Vulfson EN (2000) Imprinted polymers prepared with stoichiometric template-monomer complexes: Efficient binding of ampicillin from aqueous solutions. Macromolecules 33 (14):5098-5105. doi:10.1021/ma000467u
13. Manesiotis P, Osmani Q, McLoughlin P (2012) An enantio-selective chromatographic stationary phase for S-ibuprofen prepared by stoichiometric molecular imprinting. Journal of Materials Chemistry 22 (22):11201-11207. doi:10.1039/c2jm16659c
14. Urraca JL, Hall AJ, Moreno-Bondi MC, Sellergren B (2006) A stoichiometric molecularly imprinted polymer for the class-selective recognition of antibiotics in aqueous media. Angewandte Chemie-International Edition 45 (31):5158-5161. doi:10.1002/anie.200601636
15. Wulff G, Knorr K (2001) Stoichiometric noncovalent interaction in molecular imprinting. Bioseparation 10 (6):257-276. doi:10.1023/a:1021585518592
16. Pap T, Horvai G (2004) Binding assays with molecularly imprinted polymers - why do they work? Journal of Chromatography B-Analytical Technologies in the Biomedical and Life Sciences 804 (1):167-172
17. Baggiani C, Giovannoli C, Anfossi L, Passini C, Baravalle P, Giraudi G (2012) A Connection between the Binding Properties of Imprinted and Nonimprinted Polymers: A Change of Perspective in Molecular Imprinting. Journal of the American Chemical Society 134 (3):1513-1518. doi:10.1021/ja205632t
18. Toth B, Pap T, Horvath V, Horvai G (2006) Nonlinear adsorption isotherm as a tool for understanding and characterizing molecularly imprinted polymers. Journal of Chromatography A 1119 (1-2):29-33. doi:10.1016/j.chroma.2005.10.048

19. Toth B, Pap T, Horvath V, Horvai G (2007) Which molecularly imprinted polymer is better? Analytica Chimica Acta 591 (1):17-21. doi:10.1016/j.aca.2007.01.016
20. Castell OK, Barrow DA, Kamarudin AR, Allender CJ (2011) Current practices for describing the performance of molecularly imprinted polymers can be misleading and may be hampering the development of the field. J Mol Recognit 24 (6):1115-1122. doi:10.1002/jmr.1161
21. Castell OK, Allender CJ, Barrow DA (2006) Novel biphasic separations utilising highly selective molecularly imprinted polymers as biorecognition solvent extraction agents. Biosens Bioelectron 22 (4):526-533. doi:10.1016/j.bios.2006.07.017
22. Garcia-Calzon JA, Diaz-Garcia ME (2007) Characterization of binding sites in molecularly imprinted polymers. Sensors and Actuators B-Chemical 123 (2):1180-1194. doi:10.1016/j.snb.2006.10.068
23. Ansell RJ, Gamlien A, Berglund J, Mosbach K, Haupt K Unpublished work.
24. Norby JG, Ottolenghi P, Jensen J (1980) Scatchard plot - common misinterpretation of binding experiments. Anal Biochem 102 (2):318-320. doi:10.1016/0003-2697(80)90160-8
25. Vlatakis G, Andersson L, Müller R, Mosbach K (1993) Drug Assay Using Antibody Mimics Made by Molecular Imprinting. Nature 361 (18 feb):645-647
26. Andersson LI, Muller R, Vlatakis G, Mosbach K (1995) Mimics of the binding sites of opioid receptors obtained by molecular imprinting of enkephalin and morphine. Proceedings of the National Academy of Sciences of the United States of America 92 (11):4788-4792. doi:10.1073/pnas.92.11.4788
27. Lehmann M, Dettling M, Brunner H, Tovar GEM (2004) Affinity parameters of amino acid derivative binding to molecularly imprinted nanospheres consisting of poly (ethylene glycol dimethacrylate)-co-(methacrylic acid). Journal of Chromatography B-Analytical Technologies in the Biomedical and Life Sciences 808 (1):43-50. doi:10.1016/j.jchromb.2004.03.068
28. Li H, Nie LH, Yao SZ (2004) Adsorption isotherms and sites distribution of caffeic acid - imprinted polymer monolith from frontal analysis. Chromatographia 60 (7-8):425-431. doi:10.1365/s10337-004-0403-9
29. Sajonz P, Kele M, Zhong G, Sellergren B, Guiochon G (1998) Study of the Thermodynamics and Mass Transfer Kinetics of Two Enantiomers on a Polymeric Imprinted Stationary Phase. J Chromatogr A 810 (1-2):1-17
30. Umpleby RJ, Baxter SC, Rampey AM, Rushton GT, Chen YZ, Shimizu KD (2004) Characterization of the heterogeneous binding site affinity distributions in molecularly imprinted polymers. Journal of Chromatography B-Analytical Technologies in the Biomedical and Life Sciences 804 (1):141-149. doi:10.1016/j.jchromb.2004.01.064
31. Umpleby RJ, Baxter SC, Bode M, Berch JK, Shah RN, Shimizu KD (2001) Application of the Freundlich adsorption isotherm in the characterization of molecularly imprinted polymers. Analytica Chimica Acta 435 (1):35-42. doi:10.1016/s0003-2670(00)01211-3

32. Rampey AM, Umpleby RJ, Rushton GT, Iseman JC, Shah RN, Shimizu KD (2004) Characterization of the imprint effect and the influence of imprinting conditions on affinity, capacity, and heterogeneity in molecularly imprinted polymers using the Freundlich isotherm-affinity distribution analysis. Analytical Chemistry 76 (4):1123-1133. doi:10.1021/ac0345345
33. Rushton GT, Karns CL, Shimizu KD (2005) A critical examination of the use of the Freundlich isotherm in characterizing molecularly imprinted polymers (MLPs). Analytica Chimica Acta 528 (1):107-113. doi:10.1016/j.aca.2004.07.048
34. Umpleby RJ, Baxter SC, Chen YZ, Shah RN, Shimizu KD (2001) Characterization of molecularly imprinted polymers with the Langmuir-Freundlich isotherm. Analytical Chemistry 73 (19):4584-4591. doi:10.1021/ac0105686
35. Tamayo FG, Casillas JL, Martin-Esteban A (2003) Highly selective fenuron-imprinted polymer with a homogeneous binding site distribution prepared by precipitation polymerisation and its application to the clean-up of fenuron in plant samples. Analytica Chimica Acta 482 (2):165-173. doi:10.1016/s0003-2670(03)00213-7
36. Cacho C, Turiel E, Martin-Esteban A, Perez-Conde C, Camara C (2004) Characterisation and quality assessment of binding sites on a propazine-imprinted polymer prepared by precipitation polymerisation. Journal of Chromatography B-Analytical Technologies in the Biomedical and Life Sciences 802 (2):347-353. doi:10.1016/j.jchromb.2003.12.018
37. Turiel E, Perez-Conde C, Martin-Esteban A (2003) Assessment of the cross-reactivity and binding sites characterisation of a propazine-imprinted polymer using the Langmuir-Freundlich isotherm. Analyst 128 (2):137-141. doi:10.1039/b210712k
38. Corton E, Garcia-Calzon JA, Diaz-Garcia ME (2007) Kinetics and binding properties of cloramphenicol imprinted polymers. Journal of Non-Crystalline Solids 353 (8-10):974-980. doi:10.1016/j.jnoncrysol.2006.12.066
39. Wulff G, Grobeeinsler R, Vesper W, Sarhan A (1977) Enzyme-analogue built polymers. 5. Specificity distribution of chiral cavities prepared in synthetic polymers. Makromolekulare Chemie-Macromolecular Chemistry and Physics 178 (10):2817-2825
40. Shea KJ, Spivak DA, Sellergren B (1993) Polymer complements to nucleotide bases - selective binding of adenine-derivatives to imprinted polymers. Journal of the American Chemical Society 115 (8):3368-3369. doi:10.1021/ja00061a061
41. Guo TY, Xia YQ, Hao GJ, Song MD, Zhang BH (2004) Adsorptive separation of hemoglobin by molecularly imprinted chitosan beads. Biomaterials 25 (27):5905-5912. doi:10.1016/j.biomaterials.2004.01.032
42. Ju JY, Shin CS, Whitcombe MJ, Vulfson EN (1999) Binding properties of an aminostyrene-based polymer imprinted with glutamylated monascus pigments. Biotechnology Techniques 13 (10):665-669. doi:10.1023/a:1008955528251
43. Mathew J, Buchardt O (1995) Molecular imprinting approach for the recognition of adenine in aqueous medium and hydrolysis of adenosine 5'-triphosphate. Bioconjugate Chemistry 6 (5):524-528. doi:10.1021/bc00035a004

44. Milojkovic SS, Kostoski D, Comor JJ, Nedeljkovic JM (1997) Radiation induced synthesis of molecularly imprinted polymers. Polymer 38 (11):2853-2855. doi:10.1016/s0032-3861(97)85624-8
45. Puzio K, Delepee R, Vidal R, Agrofoglio LA (2013) Combination of computational methods, adsorption isotherms and selectivity tests for the conception of a mixed non-covalent-semi-covalent molecularly imprinted polymer of vanillin. Analytica Chimica Acta 790:47-55. doi:10.1016/j.aca.2013.06.036
46. Song D, Zhang Y, Geer MF, Shimizu KD (2014) Characterization of molecularly imprinted polymers using a new polar solvent titration method. J Mol Recognit 27 (7):448-457. doi:10.1002/jmr.2365
47. Malosse L, Palmas P, Buvat P, Adès D, Siove A (2008) Novel Stoichiometric, Noncovalent Pinacolyl Methylphosphonate Imprinted Polymers: A Rational Design by NMR Spectroscopy. Macromolecules 41 (21):7834-7842. doi:10.1021/ma801171g
48. Yilmaz E, Mosbach K, Haupt K (1999) Influence of functional and cross-linking monomers and the amount of template on the performance of molecularly imprinted polymers in binding assays. Analytical Communications 36 (5):167-170. doi:10.1039/a901339c
49. Wei ST, Molinelli A, Mizaikoff B (2006) Molecularly imprinted micro and nanospheres for the selective recognition of 17 beta-estradiol. Biosens Bioelectron 21 (10):1943-1951. doi:10.1016/j.bios.2005.09.017
50. Sellergren B (2001) Imprinted chiral stationary phases in high-performance liquid chromatography. Journal of Chromatography A 906 (1-2):227-252. doi:10.1016/s0021-9673(00)00929-8
51. Sellergren B, Lepisto M, Mosbach K (1988) Highly enantioselective and substrate-selective polymers obtained by molecular imprinting utilizing noncovalent interactions - NMR and chromatographic studies on the nature of recognition. Journal of the American Chemical Society 110 (17):5853-5860. doi:10.1021/ja00225a041
52. Lei JD, Tan TW (2002) Enantioselective separation of naproxen and investigation of affinity chromatography model using molecular imprinting. Biochemical Engineering Journal 11 (2-3):175-179. doi:10.1016/s1369-703x(02)00022-0
53. Sun RF, Yu HM, Luo H, Shen ZY (2004) Construction and application of a stoichiometric displacement model for retention in chiral recognition of molecular imprinting. Journal of Chromatography A 1055 (1-2):1-9. doi:10.1016/j.chroma.2004.08.161
54. Kuah KL, Ansell RJ. Unpublished
55. Sellergren B, Shea K (1995) Origin of peak asymmetry and the effect of temperature on solute retention in enantiomer separations on imprinted chiral stationary phases. J Chromatogr A 690:29-39
56. Kim H, Guiochon G (2005) Thermodynamic functions and intraparticle mass transfer kinetics of structural analogues of a template on molecularly imprinted polymers in liquid chromatography. Journal of Chromatography A 1097 (1-2):84-97. doi:10.1016/j.chroma.2005.08.020

57. Kim H, Kaczmarski K, Guiochon G (2005) Mass transfer kinetics on the heterogeneous binding sites of molecularly imprinted polymers. Chemical Engineering Science 60 (20):5425-5444. doi:10.1016/j.ces.2005.04.057
58. Kim H, Kaczmarski K, Guiochon G (2006) Isotherm parameters and intraparticle mass transfer kinetics on molecularly imprinted polymers in acetonitrile/buffer mobile phases. Chemical Engineering Science 61 (16):5249-5267. doi:10.1016/j.ces.2006.03.043
59. Kim H, Kaczmarski K, Guiochon G (2006) Intraparticle mass transfer kinetics on molecularly imprinted polymers of structural analogues of a template. Chemical Engineering Science 61 (4):1122-1137. doi:10.1016/j.ces.2005.08.012
60. Kim HJ, Kaczmarski K, Guiochon G (2006) Thermodynamic analysis of the heterogenous binding sites of molecularly imprinted polymers. Journal of Chromatography A 1101 (1-2):136-152. doi:10.1016/j.chroma.2005.09.092
61. Toth B, Laszlo K, Horvai G (2005) Chromatographic behavior of silica-polymer composite molecularly imprinted materials. Journal of Chromatography A 1100 (1):60-67. doi:10.1016/j.chroma.2005.09.015
62. Seebach A, Seidel-Morgenstern A (2007) Enantioseparation on molecularly imprinted monoliths - Preparation and adsorption isotherms. Analytica Chimica Acta 591 (1):57-62. doi:10.1016/j.aca.2007.02.059
63. Baggiani C, Baravalle P, Anfossi L, Tozzi C (2005) Comparison of pyrimethanil-imprinted beads and bulk polymer as stationary phase by non-linear chromatography. Analytica Chimica Acta 542 (1):125-134. doi:10.1016/j.aca.2004.10.088
64. Lee W-C, Cheng C-H, Pan H-H, Chung T-H, Hwang C-C (2008) Chromatographic characterization of molecularly imprinted polymers. Analytical and Bioanalytical Chemistry 390 (4):1101-1109. doi:10.1007/s00216-007-1765-2
65. Chaiken IM (1986) Analytical affinity chromatography in studies of molecular recognition in biology - a review. Journal of Chromatography 376:11-32. doi:10.1016/s0378-4347(00)80821-x
66. Kasai K, Oda Y, Nishikata M, Ishii S (1986) Frontal affinity chromatography - theory for its application to studies on specific interactions of biomolecules. Journal of Chromatography 376:33-47. doi:10.1016/s0378-4347(00)80822-1
67. Calleri E, Temporini C, Massolini G (2011) Frontal affinity chromatography in characterizing immobilized receptors. Journal of Pharmaceutical and Biomedical Analysis 54 (5):911-925. doi:10.1016/j.jpba.2010.11.040
68. Ramstrom O, Nicholls IA, Mosbach K (1994) Synthetic peptide receptor mimics - highly stereoselective recognition in noncovalent molecularly imprinted polymers. Tetrahedron-Asymmetry 5 (4):649-656. doi:10.1016/0957-4166(94)80027-8
69. Kempe M, Mosbach K (1991) Binding-studies on substrate- and enantio-selective molecularly imprinted polymers. Analytical Letters 24 (7):1137-1145
70. Andersson HS, KochSchmidt AC, Ohlson S, Mosbach K (1996) Study of the nature of recognition in molecularly imprinted polymers. J Mol Recognit 9 (5-6):675-682. doi:10.1002/(sici)1099-1352(199634/12)9:5/6<675::aid-jmr320>3.0.co;2-c

71. Baggiani C, Giovannoli C, Anfossi L, Tozzi C (2001) Molecularly imprinted solid-phase extraction sorbent for the clean-up of chlorinated phenoxyacids from aqueous samples. Journal of Chromatography A 938 (1-2):35-44. doi:10.1016/s0021-9673(01)01126-8
72. Baggiani C, Trotta F, Giraudi G, Moraglio G, Vanni A (1997) Chromatographic characterization of a molecularly imprinted polymer binding theophylline in aqueous buffers. Journal of Chromatography A 786 (1):23-29. doi:10.1016/s0021-9673(97)00537-2
73. Meng ZH, Zhou LM, Wang JF, Wang QH, Zhu DQ (1999) Molecule imprinting chiral stationary phase. Biomedical Chromatography 13 (6):389-393. doi:10.1002/(sici)1099-0801(199910)13:6<389::aid-bmc897>3.3.co;2-h
74. Liu HY, Yang GL, Liu SB, Wang MM, Chen Y (2005) Molecular recognition properties and adsorption isotherms of diniconaziole-imprinted polymers. Journal of Liquid Chromatography & Related Technologies 28 (15):2315-2323. doi:10.1080/10826070500187509
75. Chen YB, Kele M, Sajonz P, Sellergren B, Guiochon G (1999) Influence of thermal annealing on the thermodynamic and mass transfer kinetic properties of D- and L-phenylalanine anilide on imprinted polymeric stationary phases. Analytical Chemistry 71 (5):928-938. doi:10.1021/ac981154o
76. Szabelski P, Kaczmarski K, Cavazzini A, Chen YB, Sellergren B, Guiochon G (2002) Energetic heterogeneity of the surface of a molecularly imprinted polymer studied by high-performance liquid chromatography. Journal of Chromatography A 964 (1-2):99-111
77. Chen YB, Kele M, Quinones I, Sellergren B, Guiochon G (2001) Influence of the pH on the behavior of an imprinted polymeric stationary phase - supporting evidence for a binding site model. Journal of Chromatography A 927 (1-2):1-17
78. Kim HJ, Guiochon G (2005) Thermodynamic studies of the solvent effects in chromatography on molecularly imprinted polymers. 3. Nature of the organic mobile phase. Analytical Chemistry 77 (8):2496-2504. doi:10.1021/ac040171c
79. Kim H, Guiochon G (2005) Thermodynamic studies on the solvent effects in chromatography on molecularly imprinted polymers. 1. Nature of the organic modifier. Analytical Chemistry 77 (6):1708-1717. doi:10.1021/ac040155f
80. Kim H, Guiochon G (2005) Thermodynamic studies on solvent effects in molecularly imprinted polymers. 2. Concentration of the organic modifier. Analytical Chemistry 77 (6):1718-1726. doi:10.1021/ac040164o
81. Kim HJ, Guiochon G (2005) Comparison of the thermodynamic properties of particulate and monolithic columns of molecularly imprinted copolymers. Analytical Chemistry 77 (1):93-102. doi:10.1021/ac0401218
82. Kim H, Guiochon G (2005) Adsorption on molecularly imprinted polymers of structural analogues of a template. sing le-component adsorption isotherm data. Analytical Chemistry 77 (19):6415-6425. doi:10.1021/ac050914+
83. Miyabe K, Guiochon G (2003) Measurement of the parameters of the mass transfer kinetics in high performance liquid chromatography. Journal of Separation Science 26 (3-4):155-173. doi:10.1002/jssc.200390024

84. Chen WY, Chen CS, Lin FY (2001) Molecular recognition in imprinted polymers: thermodynamic investigation of analyte binding using microcalorimetry. Journal of Chromatography A 923 (1-2):1-6. doi:10.1016/s0021-9673(01)00971-2
85. Dvorakova G, Haschick R, Chiad K, Klapper M, Muellen K, Biffis A (2010) Molecularly Imprinted Nanospheres by Nonaqueous Emulsion Polymerization. Macromolecular Rapid Communications 31 (23):2035-2040. doi:10.1002/marc.201000406
86. Hsu C-Y, Lin H-Y, Thomas JL, Wu B-T, Chou T-C (2006) Incorporation of styrene enhances recognition of ribonuclease A by molecularly imprinted polymers. Biosens Bioelectron 22 (3):355-363. doi:10.1016/j.bios.2006.05.008
87. Kimhi O, Bianco-Peled H (2007) Study of the interactions between protein-imprinted hydrogels and their templates. Langmuir 23 (11):6329-6335. doi:10.1021/la700248s
88. Kirchner R, Seidel J, Wolf G, Wulff G (2002) Calorimetric investigation of chiral recognition processes in a molecularly imprinted polymer. Journal of Inclusion Phenomena and Macrocyclic Chemistry 43 (3-4):279-283. doi:10.1023/a:1021243826862
89. Manesiotis P, Hall AJ, Courtois J, Irgum K, Sellergren B (2005) An artificial riboflavin receptor prepared by a template analogue imprinting strategy. Angewandte Chemie-International Edition 44 (25):3902-3906. doi:10.1002/anie.200500342
90. Weber A, Dettling M, Brunner H, Tovar GEM (2002) Isothermal titration calorimetry of molecularly imprinted polymer nanospheres. Macromolecular Rapid Communications 23 (14):824-828. doi:10.1002/1521-3927(20021001)23:14<824::aid-marc824>3.0.co;2-p
91. Rick J, Chou TC (2005) Imprinting unique motifs formed from protein-protein associations. Analytica Chimica Acta 542 (1):26-31. doi:10.1016/j.aca.2004.12.051
92. Rick J, Chou TC (2005) Enthalpy changes associated with protein binding to thin films. Biosens Bioelectron 20 (9):1878-1883. doi:10.1016/j.bios.2004.11.015
93. Tamayo FG, Casillas JL, Martin-Esteban A (2005) Evaluation of new selective molecularly imprinted polymers prepared by precipitation polymerisation for the extraction of phenylurea herbicides. Journal of Chromatography A 1069 (2):173-181. doi:10.1016/j.chroma.2005.02.029
94. Duffy DJ, Das K, Hsu SL, Penelle J, Rotello VM, Stidham HD (2002) Binding efficiency and transport properties of molecularly imprinted polymer thin films. Journal of the American Chemical Society 124 (28):8290-8296. doi:10.1021/ja0201146
95. Pasetto P, Flavin K, Resmini M (2009) Simple spectroscopic method for titration of binding sites in molecularly imprinted nanogels with hydrolase activity. Biosens Bioelectron 25 (3):572-578. doi:10.1016/j.bios.2009.03.042
96. Bompart M, Gheber LA, De Wilde Y, Haupt K (2009) Direct detection of analyte binding to single molecularly imprinted polymer particles by confocal

Raman spectroscopy. Biosens Bioelectron 25 (3):568-571. doi:10.1016/j.bios.2009.01.020
97. Muk NS, Narayanaswamy R (2011) Molecularly imprinted polymers as optical sensing receptors: Correlation between analytical signals and binding isotherms. Analytica Chimica Acta 703 (2):226-233. doi:10.1016/j.aca.2011.07.032
98. Yoshikawa M, Guiver MD, Robertson GP (2008) Surface Plasmon Resonance Studies on Molecularly Imprinted Films. Journal of Applied Polymer Science 110 (5):2826-2832. doi:10.1002/app.28686
99. Diltemiz SE, Hur D, Ersoz A, Denizli A, Say R (2009) Designing of MIP based QCM sensor having thymine recognition sites based on biomimicking DNA approach. Biosens Bioelectron 25 (3):599-603. doi:10.1016/j.bios.2009.01.032
100. Diltemiz SE, Hur D, Kecili R, Ersoz A, Say R (2013) New synthesis method for 4-MAPBA monomer and using for the recognition of IgM and mannose with MIP-based QCM sensors. Analyst 138 (5):1558-1563. doi:10.1039/c2an36291k
101. El Kirat K, Bartkowski M, Haupt K (2009) Probing the recognition specificity of a protein molecularly imprinted polymer using force spectroscopy. Biosens Bioelectron 24 (8):2618-2624. doi:10.1016/j.bios.2009.01.018
102. El-Sharif HF, Hawkins DM, Stevenson D, Reddy SM (2014) Determination of protein binding affinities within hydrogel-based molecularly imprinted polymers (HydroMIPs). Physical Chemistry Chemical Physics 16 (29):15483-15489. doi:10.1039/c4cp01798f
103. Levi L, Raim V, Srebnik S (2011) A brief review of coarse-grained and other computational studies of molecularly imprinted polymers. J Mol Recognit 24 (6):883-891. doi:10.1002/jmr.1135
104. Ansell RJ, Wang D (2009) Imprinted polymers for chiral resolution of (+/-)-ephedrine. Part 3: NMR predictions and HPLC results with alternative functional monomers. Analyst 134 (3):564-576. doi:10.1039/b815145h
105. Ansell RJ, Wang D, Kuah JKL (2008) Imprinted polymers for chiral resolution of (+/-)-ephedrine. Part 2: probing pre-polymerisation equilibria in different solvents by NMR. Analyst 133 (12):1673-1683. doi:10.1039/b806376a
106. Schillinger E, Moeder M, Olsson GD, Nicholls IA, Sellergren B (2012) An Artificial Estrogen Receptor through Combinatorial Imprinting. Chemistry-a European Journal 18 (46):14773-14783. doi:10.1002/chem.201201428
107. Meier F, Schott B, Riedel D, Mizaikoff B (2012) Computational and experimental study on the influence of the porogen on the selectivity of 4-nitrophenol molecularly imprinted polymers. Analytica Chimica Acta 744:68-74. doi:10.1016/j.aca.2012.07.020
108. Denderz N, Lehotay J, Cizmarik J, Cibulkova Z, Simon P (2012) Thermodynamic study of molecularly imprinted polymer used as the stationary phase in high performance liquid chromatography. Journal of Chromatography A 1235:77-83. doi:10.1016/j.chroma.2012.02.051
109. Rosengren AM, Golker K, Karlsson JG, Nicholls IA (2009) Dielectric constants are not enough: Principal component analysis of the influence of solvent

properties on molecularly imprinted polymer-ligand rebinding. Biosens Bioelectron 25 (3):553-557. doi:10.1016/j.bios.2009.06.042
110. Andersson LI (1996) Application of molecular imprinting to the development of aqueous buffer and organic solvent based radioligand binding assays for (S)-propranolol. Analytical Chemistry 68 (1):111-117. doi:10.1021/ac950668+
111. Haupt K, Mayes AG, Mosbach K (1998) Herbicide assay using an imprinted polymer based system analogous to competitive fluoroimmunoassays. Analytical Chemistry 70 (18):3936-3939. doi:10.1021/ac980175f
112. Dong XC, Sun H, Lu XY, Wang HB, Liu SX, Wang N (2002) Separation of ephedrine stereoisomers by molecularly imprinted polymers - influence of synthetic conditions and mobile phase compositions on the chromatographic performance. Analyst 127 (11):1427-1432. doi:10.1039/b202295h
113. Sellergren B, Shea KJ (1993) Chiral ion-exchange chromatography - correlation between solute retention and a theoretical ion-exchange model using imprinted polymers. Journal of Chromatography A 654 (1):17-28. doi:10.1016/0021-9673(93)83061-v
114. Umpleby RJ, Bode M, Shimizu KD (2000) Measurement of the continuous distribution of binding sites in molecularly imprinted polymers. Analyst 125 (7):1261-1265. doi:10.1039/b002354j
115. Stanley BJ, Szabelski P, Chen YB, Sellergren B, Guiochon G (2003) Affinity distributions of a molecularly imprinted polymer calculated numerically by the expectation-maximization method. Langmuir 19 (3):772-778. doi:10.1021/la020747y
116. Wei S, Jakusch M, Mizaikoff B (2007) Investigating the mechanisms of 17 beta-estradiol imprinting by computational prediction and spectroscopic analysis. Analytical and Bioanalytical Chemistry 389 (2):423-431. doi:10.1007/s00216-007-1358-0